Technical Design of the Central Muon System

B. Baldin, E. Chi, D. Denisov, H. T. Diehl, H. Haggerty, A. S. Ito,
E. Lavallie, A. Stefanik, F. Yoffe

Fermi National Accelerator Laboratory, Batavia, IL 60510

R. Jesik, T. Marshall, A. Zieminski

Indiana University, Bloomington, IN 47405

V. Gavrilov, Y. Gershtein, V. Kolosov, S. Kuleshov, D. Litvintsev,
V. Stolin, A. Ulyanov, A. Umashev

Institute of Theoretical and Experimental Physics, RU-117259 Moscow

S. Eno, G. Gomez, N. J. Hadley, A. Lyon, J. Thompson,

University of Maryland, College Park, MD, 20742

O. Bardon, P. Hanlet, D. Wood, T. Yasuda

Northeastern University, Boston, MA 02115

D. Hedin, C. Nicholson, V. Sirotenko

Northern Illinois University, DeKalb, IL 60115

B. S. Acharya, S. Banerjee, S.R. Dugad, M.R. Krishnaswamy,
N.K. Mondal, V.S. Narasimham, N. Parua, H.C. Shankar

Tata Institute of Fundamental Research, Colaba, Bombay, 400005, India

DØNote 3365
March 29, 1997
Updated November 11, 1997
Updated March 12, 1998

Abstract

The upgraded DØ central muon detector will consist of three detector systems: the WAMUS drift chambers, the Cosmic Cap and Bottom scintillation counters, and the $A\phi$ scintillation counters. We describe the design of these detector systems.

Contents

1 Introduction **4**

2 The Central Muon Detector **5**

3 Toroid Magnet and Operation **6**

4 WAMUS Drift Chambers **6**
- 4.1 Operating Gas . . . 7
- 4.2 Radiation Damage and Aging Studies . . . 7
- 4.3 High Voltage System . . . 8
- 4.4 Mechanical Modifications . . . 9
- 4.5 Access . . . 10
- 4.6 Survey Requirements and Plan . . . 10
- 4.7 Commissioning . . . 11
- 4.8 Calibration, Monitoring, and Operation . . . 11

5 Cosmic Cap and Bottom Counters **12**
- 5.1 Cosmic Cap Counter Design . . . 12
- 5.2 Cosmic Bottom Counter Design . . . 13
- 5.3 Aging of PMTs and Scintillator . . . 14
  - 5.3.1 EMI Phototubes . . . 14
  - 5.3.2 FEU115 Phototubes . . . 15
  - 5.3.3 Scintillator and Fiber . . . 15
- 5.4 High Voltage . . . 15
- 5.5 Survey Requirements and Plan . . . 15
- 5.6 Commissioning . . . 16
- 5.7 Calibration, Monitoring, and Operation . . . 16

6 $A\phi$ Scintillation Counters **17**
- 6.1 Counter Design . . . 17
- 6.2 Prototype Counter Performance . . . 18
- 6.3 Mounting Scheme and Space Requirements . . . 18
- 6.4 Access Issues . . . 19
- 6.5 High Voltage . . . 19
- 6.6 Aging of PMTs and Scintillator . . . 20
  - 6.6.1 FEU115 Phototubes . . . 20
  - 6.6.2 Scintillator and Fiber . . . 20
- 6.7 Survey Requirements and Plan . . . 20
- 6.8 Commissioning . . . 20
- 6.9 Calibration, Monitoring, and Operation . . . 20
- 6.10 $A\phi$ Shielding . . . 21

7 Conclusion **21**

Appendix 1: Calibration and Monitoring Systems – General Description **22**

Appendix 2: Cost Estimate **23**

Appendix 3: Schedule **25**

Bibliography **27**

List of Tables

1 Channel count for the various central muon upgrade detectors. These are sorted by layer. This does not include spare counters or electronics. 5
2 Wamus aging estimates for Run I. This was the integrated luminosity required to drop the gain by e^{-1} (63%). 8
3 Location, quantity and sizes of Cosmic Cap and Cosmic Bottom scintillation counters. The Cosmic Cap counters were installed and operated during Run I. All of the scintillator is 1/2" thick. 14
4 Number and sizes of $A\phi$ counters. 17

List of Figures

1 Plan view of the upgraded muon detector. 29
2 View of the central muon toroid showing the coils, the center beam, and the seams for opening and closing the detector. 30
3 Magnetic field of the central and forward muon toroids plotted against the magnet current. 31
4 Wamus. Fig (a) is the end view of the 3-deck extrusion. Fig. (b) is the end view of the 4-deck extrusion. The larger figure shows the end view of a single cell, in cluding the cathode pad. 32
5 Wamus pads viewed from above. 32
6 Momentum resolution of the muon system compared to the SFT. Notice the fiber tracker is alway better than the central muon system. 33
7 Detail of fiber layout for the CF Cosmic Cap counter. 34
8 CF Cosmic Cap counter assembly top view. This shows the appearance of the counter as seen with the PMT cover removed. 35
9 Detail of the fiber layout for the CF Bottom B counters. 36
10 EF Bottom B counter assembly. Notice the grooves in the scintillator are oriented vertically. 37
11 Efficiency and AND rate vs. voltage for a Cosmic Cap counter operated in Run I. 38
12 Timing spectrum for prompt muons and out-of-time background in two early prototype $A\phi$ counters operated in Run I. 39
13 Layout of the A-Layer counters. 40
14 Detail drawing of the overlap of two A-Layer counters. 41
15 The design of the latest prototype $A\phi$ counter. 42

16 Amplitude spectra for Aϕ counter prototype. Solid histogram corresponds to the area along the short edge of the counter, dashed histogram - to the area in the middle of the counter. Events near zero are due to random noise in trigger counters. 43
17 Time resolution of Aϕ prototype as a function of threshold. 44
18 Relative gain change of several 115M PMT's in magnetic fields parallel to the tube axis. Open circles, squares, and triangles are with a 48 mm magnetic shield; closed circles, squares, and triangles are with a 42 mm magnetic shield. 45
19 End view of the A-Layer shield. 46
20 Side view of the A-Layer shield. 47

1 Introduction

The goal of the DØ Upgrade[1] is to exploit the physics potential to be presented by the Main Injector and Tevatron Collider during Run II. An integrated luminosity of 2 fb^{-1} is expected with instantaneous luminosity of up to 2×10^{32} $cm^{-2}s^{-1}$ accompanied by a reduction in the bunch spacing from the present $3.6\mu s$ to 396 ns, and eventually to 132 ns. This factor of 10 increase in integrated luminosity over the Run I levels will provide the opportunity for significant improvements sweeping the wide range of physics studied[2] at DØ during Run I, including precision studies of the top quark, intermediate vector bosons, QCD, new phenomena, and B-physics. In addition, important new capabilities provided by magnetic central tracking, displaced vertex tagging from a silicon strip tracker, central and forward EM preshower detectors, and improved muon detection will extend the range of high p_T physics to be studied with the DØ detector[3].

Integral to this physics is the capability to identify and trigger on muons. The muon upgrade design is driven by the observation that the proportional drift chambers used in Run I deteriorate too rapidly with integrated luminosity to be used in the forward region in Run II. Thus, an integrated solution was developed[3] that included replacement of the forward drift tubes with mini-drift tube planes, introduction of multiple planes of scintillation counters for triggering over all η, and extension of the forward muon iron absorber with additional hermetic shielding around the beampipe to reduce particle backgrounds. In the central region, we will retain the present drift tube system, complete the scintillator coverage around the outside of the toroid magnet, add an additional layer of scintillation counters in front of the toroid magnet to increase the trigger capability, and provide shielding to minimize the non-muon backgrounds.

Since the development of the conceptual design, approved by the experiment on February 1, 1996 and subsequently presented to the DoE on April 16-17, we have worked at firming up details of the design and schedule, being conscience of the need to control costs. In this report we will summarize that work to date.

The remainder of this TDR contains the following sections. Section 2 is an overview of the central muon system. Section 3 is a short description of the toroid magnet and the plan for it's operation. Section 4 is a description of the upgrade of the WAMUS PDT system including: description of the operating gas; radiation damage and aging studies; the high voltage system; mechanical modifications required; access issues; commissioning; and calibration, monitoring and operation. Section 5 is a description of the upgrade to the Cosmic Cap and Cosmic Bottom counters including: the counter designs; aging studies of the PMT's and scintillator; the high

Item	Layer		
	A	B	C
WAMUS PDT's (Drift Cells)	18 (1584)	38 (2424)	38 (2616)
Cosmic Cap Counters (PMTs)	-	16 (32)	240 (480)
Cosmic Bottom Counters (PMTS)	-	96 (192)	36 (72)
A-ϕ Counters (PMTS)	630 (630)	-	-

Table 1: Channel count for the various central muon upgrade detectors. These are sorted by layer. This does not include spare counters or electronics.

voltage; commissioning; and calibration, monitoring and operation. Section 6 describes the new $A\phi$ counters including those items mentioned above as well as access issues, and the mounting scheme and space requirements. Included is a description of the design of the $A\phi$ shielding (by the second update of this note we have predicted it won't be very helpful). The next section is the summary and conclusions. Appendix 1 describes some details of the calibration and monitoring system. Appendix 2 is the cost estimate. Appendix 3 is the schedule.

2 The Central Muon Detector

The central muon system presently consists[4] of a toroid magnet and two detector systems: 94 large drift chambers of the Wide-Angle-MUon-System (WAMUS) and 240 scintillation counters of the "Cosmic Cap". These detectors were built for Run I and will be a part of the upgrade.

The WAMUS chambers provide measurements for all muons traversing the central toroid magnet or the outer edge of the forward toroid magnet. There are three layers of chambers, one inside and two outside the toroid magnet, arranged in a barrel geometry. The chambers are constructed from extruded aluminum tubes and are of varying size with the largest being approximately 100×225 in^2. The chamber wires are oriented along the toroid magnetic field direction to provide the position of the bend coordinate for the muon momentum measurement.

The Cosmic Cap counters cover the top and sides of the central muon system. They are mounted on the outside of the outer layer of WAMUS chambers. The counters are constructed from plastic scintillator and wavelength shifting fibers. A photomultiplier readout and fast output enabled these counters to be used in the trigger during Run I as a cosmic ray veto.

For the Upgrade, we will complete the coverage of the Cosmic Cap underneath the toroid magnet by adding the 132 scintillation counters of the "Cosmic Bottom". In addition, we will add a layer of scintillation counters in between the calorimeter and toroid magnet, providing a scintillation counter tag for low-p_T muons and an improved spatial match with the fiber tracker at the hardware trigger level. Finally, inert shielding will be added to reduce the non-muon background flux.

Figure 1 shows a plan view of the upgraded detector including the WAMUS system, Cosmic Cap and Bottom, $A\phi$ counters, and inert shielding. Table 1 shows the channel count for each central muon detector system.

3 Toroid Magnet and Operation

The central (CF) toroid magnet, shown in Figure 2, is a square annulus 109 cm thick weighing 1973 metric tons. In order to allow access to the inner parts of the detector, it is built in three sections. The center-bottom section is a 150 cm wide beam, fixed to the detector platform, providing a base for the calorimeters and tracking chambers. Two C-shaped sections, which can be moved perpendicular to the centerbeam, complete the toroid. Twenty coils of ten turns each carried 2500 Amps and excited internal fields of up to 1.95 Tesla during Run I. The central toroid magnet covers the region $|\eta| \leq 1$.

We plan to operate the CF toroid in series with the EF toroid at a current of 1500 Amps. With this current, the magnetic field will be approximately 6% less than the Run I value. Figure 3 shows the magnet excitation curve for the CF and EF toriods given by a 2D simulation [5]. 1500 Amps is within the plateau region of the curve. As the primary measurement of the muon momentum comes from the central tracking system, we feel that the cost savings, $\sim$ \$75K per year, of operating the magnets at the reduced current more than overcomes the small loss in muon system momentum resolution. The SAMUS magnet will not be powered during Run II. The SAMUS power supply has been donated to the superconduction solenoid magnet.

A modification to the bottom section of the two halves of the magnet is discussed in detail in Section 4.4.

4 WAMUS Drift Chambers

The WAMUS central region consists of three layers of drift chambers, one layer inside and two layers outside the central toroid magnet. The purpose is to provide muon identification and a momentum measurement independent of the central tracking. Approximately 55% of the central region is covered by three layers of PDT's, close to 90% is covered by at least two layers. The drift chambers (PDT's) are large, typically 100×220 in.^{2}, and made of rectangular extruded aluminum tubes. The PDT's outside the toroid magnet have three decks of drift cells; the layer inside the toroid has four decks with the exception of the A-Layer bottom PDT's (these have 3 decks). The cells are 10.1 cm across, with typically 24 columns of cells per chamber. Figure 4 shows a cutaway view of the 3-deck and 4-deck extrusions as well as an end view of a drift tube showing the wire and vernier pads. Figure 5 shows the pad pattern which repeats every 24 inches.

The drift chambers produce the following measurements for each hit: the drift-time T to the anode wire, the difference ΔT in the arrival time of the hit between a hit cell and the neighbor connected to it at the far end, providing the distance along the wire, and the charge deposition on inner and outer vernier pads, providing a more accurate measure of the distance in the direction along the wire. The drift distance resolution will be $\sim$ 500 microns. The resolution of the ΔT measurement varies depending on whether the muon passes through the cell close to or far from the electronics. If the hit occurs far from the electronics, the resolution is approximately 10 cm. If close, the dispersion of the wire signal which propagates two wire lengths, causes the resolution to degrade to 50 cm. The using charge division, the pad signal resolution is about 5 mm. The muon momentum resolution is expected to be $\sigma(1/p) = 0.18(p-2)/p^2 \otimes 0.005$ (p in GeV/c). That is shown in Figure 6 in comparison with a central tracking system with resolution $\delta p_T = 0.0015 p_T^2$. The muon momentum resolution in the figure has separate upper and lower error bars because the uncertainty is in $1/p$. One can see that the uncertainty from the muon

system is comparable to the central tracking chamber for very high p_T muons.

We will instrument the pad readout for the whole A-Layer in order to provide the precise non-bend view measurement for matching with inner tracker tracks. We will instrument only about 10% of the pad readout in the B and C-Layers in order to monitor the PDT gains (see Section 4.2).

4.1 Operating Gas

In order to reduce the number of crossings which occur during one drift interval, we need to use a fast gas during Run II. We will operate the chambers with a non-flammable gas mixture of 80% argon, 10% methane and 10% CF_4. The operating HV will be approximately 2.5 KV for the pads and 5.0 KV for the wires. The drift velocity with these voltages is $\sim$ 10 cm per μs, for a maximum drift time of $\sim$ 500 ns. The contribution to the hit uncertainty due to diffusion is estimated as about 375 microns, worse than the present 300 microns achieved with a slower gas[6]. The trade-off in resolution is offset by the reduced occupancy and benefits to triggering achieved by decreasing the number of crossings in one drift time to 2 for 396 ns bunch spacing and 4 for 132 ns bunch spacing.

The HV operating point will depend on the sensitivity of the preamps. We will operate the chambers with as low a gain as possible in order to minimize the aging. In Run I we operated the chambers with a threshold of about 0.75μA; this varied some from PDT to PDT.

If we operated the PDT's at a gas flow rate equivalent to that used in Run I, the gas flow rate would be about 100 liters per hour. We plan to increase the flow rate by a factor of 4 to 10 because we believe the concentration of contaminant in the gas may be reduced with a higher flow rate. We studied the gas system and found no impediments to increasing the flow rate.

We will recirculate the gas in order to save on operating costs. The gas becomes contaminated in passing through the PDT's. We will need to operate a filter or cold-trap to remove the contamination. In Run I we used a refridgerator with an operating point of -70 degrees F. This "SO-LOW Ultracold Freezer" cost about \$1500. Tests during Run I showed it removed essentially all of the contaminant. We will replace it for Run II because we have concerns about its reliability. Otherwise we will use much of the gas system that was used in Run I. We will monitor the differential pressure between each PDT's input and output gas ports. A new gas block will be used. It will be smaller and simpler. We will also replace the PVC manifolds with copper ones.

4.2 Radiation Damage and Aging Studies

The WAMUS chambers undergo a fast aging when operated in a radiation environment. Vapors from a glue used in the construction of the cathode pads is deposited on the wires in a sheath with the amount of deposition proportional to the integrated charge accumulated. As the coating increases in thickness, the gain of the chamber drops and the chamber becomes inefficient. Table 4.2 shows the amount of integrated luminosity which drops the PDT gain by e^{-1} (63%). Note that we have a small plateau, so even a 25% drop in the gain, which occurs after 29% of the lifetime, will result in some loss of efficiency.

There is some indication that the aging on the East side is faster than the aging on the West in the B and C-Layer chambers of the Rings. This could be a result of the eastward offset of the Tevatron tunnel. However in a test to determine the source of the aging, when the beams were

PDT Location	Run I Lifetime (pb^{-1})
A-Layer	670
B-Layer Ring	950
B-Layer Sides, Top and Bottom	2100
C-Layer Ring	230
C-Layer Sides and Top	1560
C-Layer Bottom	4500

Table 2: Wamus aging estimates for Run I. This was the integrated luminosity required to drop the gain by e^{-1} (63%).

separated at DØ (the collisions stopped), the current draw in the chambers stopped. This would be inconsistent with background from the tunnel unless the presence of collisions at DØ caused it.

Also, there are some regions where the $Z-$dependence of the aging was important due to exposure to increased background flux. These included the outside edges of the A-layer, where the aging was about 5 times faster than the average, and the edges of the C-layer Ring, with a similar problem.

There are some mitigating factors which will substantially extend the PDT lifetime in Run II. First, we will shield the PDT's from the backgrounds. This will increase the lifetime a factor of 4 along the edge of the A-Layer. The worst parts of the ring PDT's should be improved by a factor of 50-100. Second, we will remove the contaminant via the cold trap in the recirculating gas system; however, as the source is the chambers themselves, this doesn't prevent the aging entirely. Third, we believe the aging rate may be reduced by the increased gas flow rate. Lastly, operating the chambers at a 4X lower gain will increase the lifetime by the same factor.

Despite all of the efforts, the aging will continue to occur. We will monitor the aging by using the gain determined from the sum of the inner and outer pad signals. That is the principal reason why the B and C-Layer PDT's have the 10% pad readout. The gain measurement will be a regular part of the online monitoring and also will be available in the DAQ_Local procedure. Fortunately, we have a way[7] of cleaning the wires once damage occurs. We disconnect the service cards from the front-end electronics and remove the cell-cell jumper wires on the jumper boards. We discharge a capacitor on one end of the wire while the other end is grounded. The wire heats up and the coating falls away as if peeled off. The safety of the procedure has been improved each time we perform it. We now believe it is completely safe. We plan to clean the chambers as necessary.

4.3 High Voltage System

A detailed description of the DØ high voltage and VME control is available[4]. In short, the controls system determines the HV output of the pods which reside in VME crates in the 1st floor of the Movable Counting House (MCH). Each crate can hold 48 pods. Each pod has one SHV output. The outputs from pods are then fanned-in to multi-HV conductors which we call Reynolds cables, after the manufacturer. Each Reynold cable has eight conductors. At the platform, the Reynolds cables are then fanned-out to the individual detectors via SHV cable.

The WAMUS PDT's require two HV levels, 2.5 KV for the pads and 5.0 KV for the wires.

We plan to use two crates with 47 pods each for Run II. This allows us to power two chambers from each pod and provides a monitor of two PDT's in parallel. The HV pods and the two crates which we used during Run I will be sufficient. These could provide the necessary HV at up to 3 mA. We will need to add two fan-ins in the MCH (we have sufficient spares), reroute some of the old EF Reynolds cables to the CF truss, and add some Reynolds fan-outs to the patch crates in the CF truss.

The two HV levels are distributed onto the cells through the service cards. The end service card has a daughter card with solder connections for the HV cable ends. A detailed write-up on the service cards is under preparation[8].

4.4 Mechanical Modifications

We understand we will have to make minor mechanical modifications to various parts of the WAMUS system, particularly to accomodate scintillation counters. We plan to put the Bottom C-Layer scintillator underneath their respective eight PDT's. This requires elevating slightly each of the PDT's. The electronics, which previously was on top of the PDT's, may have to be moved to the outside edge. The CF Bottom B-Layer counters have to be raised to accomodate the scintillation counters which hang underneath them[10]. The electronics will fit under or next-to the scintillation counters.

We need to increase the space between the ends of the vertically mounted B and C-layer PDT's (40) to increase the accessiblility of the service cards and jumper boards. The lower PDT's will be lowered by 1.5". The upper PDT's will be lowered 0.75".

We will have to replace the 4-deck WAMUS A-Layer PDT's on the bottom with refurbished 3-Deck PDT's discarded from the old EF WAMUS system. This is necessary because the space presently available for the bottom $A\phi$ counters is not sufficient. The use of a 3-deck PDT will provide two more inches of space, sufficient for the scintillation counters. As we do not have any 3-deck chambers of the appropriate length, we have developed a procedure for cutting a long chamber to the right size. It is possible to replace the Glassteel pads with copper clad G-10 left over from the calorimeter assembly as part of the procedure. This will largely solve the aging problem for those PDT's.

We will lower the A-Layer wall PDT's by 3/8" to make it easier to roll the A-Layer top PDT's into position. The electronics for the A-Layer wall PDT's will reside on the A-Layer bottom PDT's. The A-Layer bottom PDT's will be oriented so that their electronics is on the side away from the walls. We will change the covers used to protect the on-chamber electronics to a modular design which provides more protection.

The clear fibers which carry the light from the scintillating fiber tracker to the VLPCs on the platform penetrate the toroid magnet in the neighborhood of the CF Bottom B-Layer PDT's. In order to minimize the length of these clear fibers, it is necessary to relocate the PDT's inner edge approximately 39" further from the centerbeam compared to their Run I position. Regardless of the PDT's length, a 78" wide gap is introduced in the B-Layer PDT coverage in the downward direction, coincident with the hole in the A-Layer bottom. This hole is the reason for the CF-Bottom B-layer scintillation counters. We anticipate replacing the 183" long PDT's with shortened PDT's to ease access to the jumper board ends of the vertical PDT's just above them and to provide this gap for the tracker fibers. Two notches on each side of the toroid, next to the center beam, must be widened and deepened to 6" $\times$ 20" from the present 3" $\times$ 10" to accomodate the fiber tracker optical fibers. We studied the increased fringe field due to changing the size of

this notch and found it acceptable.

4.5 Access

We anticipate the need to access all of the WAMUS PDT's and their components. The front-end electronics, service cards and jumper boards will need repair or replacement from time-to-time. In addition, we will need to access the jumper boards and service cards in order to perform the chamber cleaning procedure. For most WAMUS chambers access is relatively easy from the muon trusses or from the calorimeter; however, some require special procedures. Here we only discuss the access to PDT's where access is non-trivial. The Bottom C-Layer counters (8) require rolling out to access the front-end electronics. The jumper boards will be inaccessible unless PDT's are removed. This is something which cannot be done in the collision hall; we do not anticipate it will be required in Run II. The access to the CF Bottom B-Layer PDT's jumper boards is difficult because of a cable tray in close proximity. The cable tray, which holds muon cables, will be moved eight inches. The Top C-Layer PDT (10) jumper boards are accessed from outside of the muon trusses. These require some kind of catwalk on the outside of the detector. We had a temporary movable platform during Run I for these PDT's. That would be sufficient. The Bottom (6) and Top (6) A-Layer PDT's must be rolled to access their jumper boards; that provides access to the Side (6) A-Layer PDT's as well. The Top A-Layer front end electronics are accessed from the East and West calorimeter platforms. All access to the A-Layer requires the CF toroid be in the open position.

There may be minor modifications to the first level of the muon truss depending on the final locations of the front-end crates for the scintillation counters. We would like to replace the plywood false floor on top of the east side PDT patch panel with an aluminum false floor in order to provide more protection for the cables.

4.6 Survey Requirements and Plan

We require knowledge of the WAMUS PDT's position to 1.0 mm in order to obtain the resolution of Figure 6. A three stage survey procedure which accomplished this for Run I was developed[21]. Phase I is the initial survey of the PDT's and references tooling balls placed on the PDT relative to the wire positions. Phase II is a global survey of a set of PDT's mounted on each piece of muon magnet iron with respect to each other. Phase III is the final measurement, made in the collision hall, which references the position of the groups of PDT's relative to each other and to the other detector systems.

All of the WAMUS PDT's have undergone a Phase I survey. However, for the first 26 PDT's surveyed, it was incorrectly assumed that the PDT's were rectangular. Of course they aren't and the deviation from rectangular is as much as 1/2 cm with an average of 1 mm. This mistake translates directly into drift direction measurement error. Unfortunately, access to the ends and sides of the PDT's is required in order to perform the Phase I survey. Fortunately, it happens that many of the poorly surveyed PDT's are temporarily removed from the detector. Chambers 11, 21, 31, 12, 32, 35, 114, 132, 134, 145, 146, 214, 232, 234, the 4 CF Bottom B-Layer PDT's, and the 8 CF Bottom C-Layer PDT's all had a poor Phase I survey. In addition to the resurvey, there are a number of PDT's with broken tooling balls. These must be replaced and surveyed in place.

The Phase II survey will have to be repeated for a large part of the WAMUS detector. All

of the Bottom B and Bottom C-Layers, the Top EF C-Layers, and all of the A-Layer, and many other PDT's will have been moved or removed. It is necessary to redo the Phase II survey; this is most easily carried out before roll-in. Herm Stredde and Andy Stefanik will see if the muon trusses "stiffness" can be improved so that a Phase II survey carried out with the detector rolled-out will still apply when the detector has been moved into the collision hall. In principal a Phase II survey would have to be repeated each time the PDT's are moved; however, so long as the direction of motion was parallel to the wires, it will be sufficient to reposition the PDT's with stops.

Some of the tooling balls important to the Phase II survey will have been covered by (removable) scintillation counters. Rather than removing and replacing the counters for the survey, we will make some simple survey transfer fixtures which allow for an in-place measurement. The tooling balls on the A-Layer PDT's will have to be moved out of the way of the new scintillation counters. Additional tooling balls will be installed in new locations to make these measurements easier to perform.

The Phase III survey must be repeated with each opening/closing of the detector. A quick analysis of the the survey data is required so that the up-to-date chamber positions can be used in the software trigger and reconstruction. During Run I this quick turn-around was sometimes complicated because the Phase II survey was compromised when the detector was opened or closed. We will do simple things such as spray-painting the chamber mounts so that those occasional instances will be easier to analyze.

4.7 Commissioning

The job of integrating the sub-systems, including HV, gas-flow, cable check-out, electronics, calibration systems, and monitoring programs officially begins on September 14, 1998 when we are scheduled (see Appendix 3) to begin the commissioning of 10% of the counters over an eight week period. The late date is chosen because it is the scheduled arrival date of the front-end electronics. In fact, this job will start sooner with the more low-level subsystems mentioned above.

The remainder of the commissioning will take place from March 16, 1999 to September 16, 1999. The last counters to be commissioned will be the CFB and CFC bottom east PDT's, installed after the detector has moved partway west.

4.8 Calibration, Monitoring, and Operation

We plan to monitor PDT characteristics with a variety of techniques. Certain characteristics, such as the gas flow, the LVPS levels, and threshold setting and readback will be monitored over the 1553 connection to the control board on the PDT's and plugged into the DØ alarm system. The HV level and current-draw of each pair of PDT's will be monitored and recorded through the HV system. Checking the current-draw against the luminosity provides a direct test of the integrity of HV to the PDT's and an indirect test of the luminosity and gain.

We will monitor and calibrate the front-end and readout electronics with four levels of DAQ. The system is described in general terms in Appendix 1.

Regular (usually weekly) calibration runs test the front-end electronics and readout. Controllable electronics pulsers on the front-end cards mimic the signals. The calibration program controls the pulser and initiates the event readout through the full trigger and data aquisition

system. The result is a bad channel (if any) list, a set of calibration constants and a comparison with the previous measurements so that any changes can be tracked. We expect this will be especially important for the A-Layer PDT's, where we have to calibrate the ADC's which readout the pads. This involves a pedestal and gain measurement. The wires will be read out with TMC TDC's and will require t_0 calibration.

A new DAQ_Local program will allow us to study individual PDT's in detail using cosmic rays or prompt beam muons. During Run I we used this program to test the electronics, cross-check the results of the calibration program, and monitor the characteristics of individual cells. This program was extremely efficient for studing individual chambers because of it's speed and extremely flexible because it didn't carry the overhead of the trigger and data aquisition system.

Lastly, in the course of normal data-taking, we will monitor the PDT's operation by producing histograms of the hits in each PDT. We also will periodically test the gain of the PDT's to monitor aging (as discussed in 4.2) by checking the sum of the pad pulse heights for muons produced by $p\bar{p}$ collisions and from cosmic rays. Of course, this will be available only for those channels that have the ADC readout.

5 Cosmic Cap and Bottom Counters

The "Cosmic Cap" scintillation counters presently cover the top and sides of the WAMUS C-Layer. Their purpose is to provide a fast trigger detector outside the toroid magnet for identifying muons from cosmic rays. The Cosmic Cap was used in the Run I muon trigger where a WAMUS trigger was accepted if the scintillation counters, where available, had a hit within a 50 ns wide gate around the expected time-of-arrival of a beam muon. A resolution of 2.5 ns was achieved after offline corrections (online, the counters have a timing resolution of about 5 ns). These will be a part of the muon trigger during Run II. In addition, during Run II, these counters will provide a timestamp for muons which pass through the WAMUS PDT's in order to tag in which crossing the muons occurred. These counters have three sizes depending on the size of the WAMUS chamber on which they are mounted. There are 12 divisions in ϕ and 20 divisions in η with the long counter dimension along ϕ.

The Cosmic Bottom counters are being built for the Bottom B and C-Layers. These counters complete the coverage of Cosmic Cap and will serve the same purpose in Run II. They provide a fast trigger element with good timing resolution outside the muon toroid and they tag the crossing for WAMUS chamber hits. The Cosmic Bottom counters will be located underneath the CF B-layer (on PDT's 115, 135, 116, and 136), underneath the EF B-layer (on PDT's 105, 106, 145, and 146), and underneath the edge of the CF C-Layer (on PDT's 205, 206, 245, and 246). The CF Side B-layer counters are located on the low sides of octants 4 and 7. The CF Bottom B-layer gap counters are located in the B-layer directly below the calorimeter centerbeam. Even though the PDT names are similar there is little overlap between the different layers.

5.1 Cosmic Cap Counter Design

The Cosmic Cap counters have been described in great detail in a draft of a NIM article[9]. They are made from grooved 0.5" Bicron 404a scintillator material with BCF 91a and Kuraray Y11 waveshifter fibers glued into the grooves using Bicron 600 Optical epoxy. The grooves are approximately one mm deep and 4 mm across. Fully 50% of the counter surface is covered with

fibers. Each fiber covers half the length of the counter. The fibers are glued with Five-Minute-Epoxy (FME) at the ends of the counters, which are then polished using a diamond cutter. In order to increase the light yield, a 1/32 inch anodized aluminum sheet is held on the ends with aluminized mylar tape. The sides of the counters are milled. The fibers are gathered at the center, divided into two bundles, and epoxied with FME into two acrylic plastic cookies with holes in the center of each. The ends of the cookies were rough cut and then polished with the diamond cutter. Figure 7 shows the fiber layout for a Cosmic Cap counter.

The Bicron scintillator is wrapped in a layer of TYVEK sheet with a hole cut for the fibers and cookies. The TYVEK wrap yields $\sim$ 10% more light than an aluminum foil or aluminized mylar wrap. A layer of 1/8 inch thick styrofoam is placed over the fibers on the counter top. Aluminum sheets 0.020" thick cover the bottom and top surfaces. An opening is left in the top sheet for the fibers and cookies and around the hole is an aluminum angle bracket lip. The aluminum sheets are taped together around the perimeter of the counter. An outer frame of Unistrut provides support for the counter. A black molded-plastic piece fits over the outside of the aluminum lip. This covers the phototubes, cookies and fibers. It is held in place with Velcro and the seams are taped with black photographic tape. The HV and BNC connector feed through this cover. Figure 8 shows the counter assembly including the phototubes and frame.

The fibers are read out with two 1.5 inch 10-stage EMI 9902KA phototubes operated in coincidence. The light yield varies depending on the distance from the phototube and the proximity to the edge. It is typically 30 photoelectrons per PMT for hits near the PMTs and 18 photoelectrons per PMT for hits near the far corners. The location, numbers of counters and sizes are summarized in Table 3. The Cosmic Cap counters were 98% efficient in Run Ib.

5.2 Cosmic Bottom Counter Design

The scintillator coverage of the region outside the toroid magnet will be completed by the Cosmic Bottom counters[10]. These are new counters for Run II. There will 132 counters, each read out by two PMTs. We use two designs for these counters. The first, shown in Figure 9 is used for the 48 CF Bottom B-Layer counters. It is nearly identical in design to the Cosmic Cap counters, using the same scintillator and fiber in shallow, wide grooves. There are some minor improvements in the fiber placement for the edge fibers made to increase the light yield. The CF-Bottom B-Layer counters use EMI 9902KA PMTs left over from the Cosmic Cap construction. The counter frames are made from 1/8" steel bent into U-shaped channels which are then bolted together, instead of Unistrut, to provide a thinner profile over the counter length. The counters are suspended from the strong edges of the CFB Bottom WAMUS PDT's. The CF Side B-layer counters are of a similar design [11].

The design of the EF Bottom B-Layer and CF Bottom C-Layer counters is similar to the Cosmic Cap counters except that the counters have fewer fibers. This is accomplished, with no loss in light yield, by placing fibers in vertical grooves approximately 6 mm deep and 6-10 cm apart instead of in the horizontal grooves of Figure 9. The light yield does not depend strongly on the separation of the grooves over that range of separations. See Figure 10 which shows a cut-away end view of an EF Bottom B-Layer counter including the scintillator and grooves, the PMTs and mounts, and the molded plastic cover and frame. The EFB Bottom counters will be suspended from the strong edges of the EFB Bottom PDT's. The CFC Bottom counters will roll underneath the CFC Bottom PDT's with one set of wheels in a track or guide so as to maintain the counter position. The 68 EFB and CFC Bottom counters will use the MELZ FEU-115, a

Location	Quantity	Width (in.)	Length (in.)	PMT
Cosmic Cap Top	80	25	113	EMI
Cosmic Cap Upper Sides	80	25	108	EMI
Cosmic Cap Lower Sides	80	25	81.5	EMI
CF Side B	12	35	49	EMI
CF Side B	4	35	67	EMI
CF Bottom B-Layer	20	22 3/8	98 1/8	EMI
CF Bottom B-Layer	20	15 3/4	98 1/8	EMI
CF Bottom B-Layer Gap	8	18 1/2	99 1/2	EMI
EF Bottom B-Layer	20	13 3/8	91 1/16	MELZ
EF Bottom B-Layer	12	19 1/4	91 1/16	MELZ
CF Bottom C-Layer	20	22 1/16	68 1/16	MELZ
CF Bottom C-Layer	16	29 3/10	68 1/16	MELZ

Table 3: Location, quantity and sizes of Cosmic Cap and Cosmic Bottom scintillation counters. The Cosmic Cap counters were installed and operated during Run I. All of the scintillator is 1/2" thick.

one inch diameter PMT. This is a 12-stage tube with 2 ns risetime and good quantum efficiency and uniformity [12]. We will use a 42 mm diameter magnetic shield. This is sufficient to protect the PMT's from the small magnetic fields expected at the location of the EFB and CFC Bottom counters.

One important difference between the Cosmic Cap and Cosmic Bottom is that the orientation of the bottom counters has the narrow dimension along phi and the long dimension along η. This orientation is preferred because it has better matching in ϕ with the inner tracking chamber trigger. The widths are selected to be approximately 4 1/2 degrees in ϕ. They are as long or slightly longer than their respective WAMUS PDT's are wide. Table 3 shows the location, number and sizes of the Cosmic Bottom scintillation counters as well as the Cosmic Cap.

5.3 Aging of PMTs and Scintillator

5.3.1 EMI Phototubes

Early in Run Ib we discovered that the EMI 9902KA PMTs underwent a gain drop depending on the integrated charge. This was studied in detail[13]. In summary, for the first 20 Coulombs of anode current the gain drops linearly to 60 or 70% of the out-of-box gain. After that the gain drops more slowly. After 300 Coulombs of anode current the gain was down to 50%. This is attributed to aging of the CsSb dynodes. Therefore, we have to take care to minimize the operating gain and avoid unnecessarily aging the PMTs.

We will run the PMTs at a gain so that we use a 5-10 mV threshold for detecting the muons. We expect the rate in the hottest Cosmic Cap counter to be approximately 100 Khz when the beam intensity is 2×10^{32} cm^{-2}s^{-1}; this corresponds to an integrated anode current of 30 to 40 Coulombs during a 2 fb^{-1} run. The Cosmic Cap PMTs mounted on the edge of the EF toroid magnet were operated in Run I and have already undergone the first 20 Coulombs of aging, so they will be fairly stable. The CF Cosmic Bottom B-Layer PMTs will have new tubes and therefore, will be subject to the fast aging. We will monitor the tubes using the ADC readout.

Also, we have the option to stabilize the aging by pulsing them with the calibration LEDs and to adjust the HV or thresholds to overcome any drop in gain.

5.3.2 FEU115 Phototubes

Detailed studies of aging *vs* integrated anode charge have been carried out for the forward muon trigger detectors, which use close to 5000 FEU115 phototubes [14]. With the Run II dose, expected to deposit less than 100 C or charge, the gain will change by less than 10%. It will be easy to adjust thresholds or HV levels to accomodate this small change. We will monitor the gain as discussed in Section 5.7.

5.3.3 Scintillator and Fiber

The radiation dose expected in the cosmic cap counters for Run II is $O(10)$ rads, based on the rate measurements taken during Run I. Measurements were made of the effect of radiation on the gain and attenuation length of Bicron 404a and both BCF 91a and BCF 92 waveshifter fiber[15]. After 20 krad, the light output from a small counter made from Bicron 404a plus BCF91a (BCF92) fiber had decreased by 1% (15%) indicating that BCF92 fiber is more sensitive to high levels of radiation than BCF91a. The attenuation length of both kinds of fibers decreased, as well. For a 110 cm long fiber made from BCF91a (BCF92), the light yield fell 25% (35%) in 20 krad. These factors should be taken as independent in calculating the total change in light yield. Obviously 20 krad is a factor of 2000 higher than the expected dose. Nevertheless, we will monitor the radiation damage to the scintillator and fiber by leaving some test samples (which can be periodically removed and measured) in the detector.

5.4 High Voltage

The Cosmic Cap occupied two HV crates with four spare slots during Run I. The 480 counters were powered by 60 Type 4 pods (2KV 2500 μA limit). The base current for the EMI 9902 is 200 μA and the expected maximum rate will contribute less than 2% more. Therefore we plan to leave the Cosmic Cap HV as is, including the fan-ins in MCH1, the Reynolds cables and the fanouts on the platform.

We have 96 EMI PMTs and 136 Melz PMTs in the Cosmic Bottom. We will power the EMI tubes using 12 more Type 4 pods in 2 of the spare slots. The Melz tubes require 150 μA each, we will use 11 Type 4 pods with 12 or 13 PMTs powered from each. The remaining pod will be used as a spare. We need 2 4X fan-ins or 3 2X fan-ins for the counting house, 6 Reynolds cables plus equivalent spares, and Reynolds to SHV fanouts in the N, S, E and W trusses. The counting house parts and Reynolds cables will be scavenged from the Run I tracking system. We will produce the Reynolds to SHV fanouts.

5.5 Survey Requirements and Plan

For the Cosmic Cap and Bottom scintillation counters, the mounting system will ensure that the counters relative positions are fixed to within about 1/8". We will reinspect them to ensure the counters are mounted properly. We will measure the position of each counter to 1/8" accuracy.

5.6 Commissioning

The job of integrating the sub-systems, including HV, cable check-out, electronics, calibration systems, and monitoring programs officially begins on October 1, 1998 when we are scheduled (see Appendix 3) to begin the commissioning of 10% of the Cosmic Cap counters and all of the bottom west counters over a 12 week period. The late date is chosen because it is the scheduled arrival date of the front-end electronics. In fact, this job will start sooner with the more low-level subsystems mentioned above.

The remainder of the commissioning will take place from February 11, 1999 to August 13, 1999. The last counters to be commissioned will be the east side CFB and CFC bottom counters, installed after the detector has moved partway west.

5.7 Calibration, Monitoring, and Operation

The performance of the Cosmic Cap and Bottom will be monitored on a regular basis. A variety of techniques were developed and used during Run I operation of the Cosmic Cap and updated versions of these will be available during Run II. Also, the addition of an LED pulser system and the use of digital signal preprocessors (DSPs) will provide powerful new capabilities. In this subsection, we describe our plans, in order of the complexity fraction of the DAQ system required, with the simplest first.

During Run I, the voltages and currents of the high voltage supplies were monitored regularly during "quiet time" between Tevatron stores. The ratio of voltage divided by current was checked for consistency over time in order to determine if any HV channels might have drifted due to moisture having been absorbed into the voltage feedback resistor. This monitor was sensitive to drifts of 10 volts or greater.

The daily 30 minute quiet time where there is no beam in the accelerator, the AND rates for each of the scintillation counters was recorded by a software program which uses the trigger board 1553 bus to selectively disable and enable counters and also place them in the "transparent mode" where the discriminator signals are ungated. The AND rate for fully efficient counters was dominated by the background photons from the collision hall walls and ceiling. By maintaining the rates at the appropriate level, we could insure that the counters were fully efficient. Periodically we lowered the thresholds for counters which were beginning to record a low AND rate to maintain full efficiency. The efficiency verses voltage for a prototype counter placed in the collision hall is shown in Figure 11 and also shown is the AND rate for the same counter.

The scintillation counter systems will use a "Daq_Local" program similar to that described above for the WAMUS system. The utility of this program is that it allows us to focus on individual counters for detailed study. It does not require the trigger framework and requires only parts of the DAQ. But it does record "mini-events" onto the host computers for further study.

The calibration program, which requires the full DAQ and trigger system, will perform three main tests. First, by pusling the front-ends, we determine if the electronics is live. Second, the TMCTEG TDS's will need t_0 calibrations and a means to monitor their stability. Finally, each grounp of 16 channels will be multiplexed to an ADC which will require the determination of a pedestal and gain constant. Calibrating these ADC's allows us to monitor the PMT gains and light yields.

As during Run I, the counters will be monitored by an online program (Examine) during

Number	Length (inches)	Width (inches)
216	33 1/4	14.46
144	33 1/4	10.84
270	33 1/4	9.090

Table 4: Number and sizes of $A\phi$ counters.

each data taking run. The program generated plots of the number of times each scintillator fired and the time distribution of the hits within gate during each run. The plots were then scanned for gross anomalies by the detector shifters at runtime and more carefully by the system experts daily.

6 $A\phi$ Scintillation Counters

The $A\phi$ counters will cover the WAMUS PDT's mounted between the calorimeter and toroid magnet. The $A\phi$ counters will provide a fast detector for triggering–on and identifying muons and for rejecting out-of-time backscatter from the forward direction. Matching in–time scintillation counter hits with tracks in the SFT at Level 1 will provide a unprescaled high-p_T single muon and low-p_T dimuon triggers. This is accomplished with timing resolution less than 4 ns at the trigger level and less than 2.5 ns offline. The phi segmentation is $\sim$ 4.5 degrees, appropriate for the expected multiple scattering for high-p_T muons. The longitudinal segmentation is 33 1/4", with a length appropriate to the necessary time resolution and matching well to the size of the WAMUS PDT's. In addition, these counters provide the timestamp for muons which pass through the WAMUS PDT's, particularly important for the low-p_T muons which do not penetrate to the Cosmic Cap or Bottom counters. Figure 12 shows the time-of-arrival of prompt muons and out-of-time backgrounds in early prototype versions operated during Run I.

There will be three counter sizes accomodating approximately a constant 4.5 deg angular coverage for each counter. The larger counters are in the corners. The arrangement in the ϕ direction on the sides of the A-Layer is three wide, three medium, eight narrow, three medium and three wide counters. For the bottom, the arrangement is three wide, one medium, two narrow, one medium, and three wide counters, with a large gap underneath the calorimeter between the sets of narrow counters. For the top it is 3 wide, 1 medium, 12 small, 1 medium, and 3 wide counters. Figure 13 shows the layout of the counters. The counters overlap in phi to reduce inefficiency due to muons which escape through cracks. Figure 14 shows detail of the overlap between $A\phi$ counters in neighboring phi slices. The average overlap between counters is about 3%. The counters are butted end-to-end with a small gap in between each. Table 4 indicates the number of counters of each size.

6.1 Counter Design

The design of the counters and cases is similar for all three sizes. They are made from Bicron 404a scintillator with G2 fiber embedded in vertical grooves in a manner similar to the EFB and CFC Cosmic Bottom counters. The grooves are $\sim$ 1.75 inches apart and run from the edge of the counter to the middle. Six fibers are spot-glued into each groove and taper out of the groove at

the middle of the counter. The fibers are routed to an FEU-115 which is secured to the counter case. All the fibers are within two inches of being the same length. The counter and fibers are wrapped in a layer of TYVEK, held on with tape. We will use a layer of black TEDLAR over the TYVEK. Figure 15 shows the design of the latest prototype counter.

The counter case is to be made from aluminum in a "shirt-box" design with welded corners. It will look similar to the prototype case shown in Fig. 15. The case provides mechanical protection, support of the PMT and counter mounts, and protection against light leaks.

6.2 Prototype Counter Performance

The performance of the Aϕ counter prototype was studied with cosmic rays. Figure 16 shows the amplitude spectra (in numbers of photoelectrons detected) for two areas of the counter: close to the short edge of the counter (furthest from the phototube) and exactly in the middle (close to the phototube). One expects the signals from the middle of the counter to be larger because collected light has to travel through less fiber and is therefore less attenuated. Light attenuation in fiber is considered to be the largest source of non-uniformity in the counter; however, the magnitude of the difference is rather small. Figure 16 shows the counter is uniform to $\pm 7\%$ level.

The time resolution was measured for different thresholds and is shown in Fig. 17. Note that the amplitude of one photoelectron in these tests was about 5 mV.

The counters will operate in the residual magnetic fields of the muon toroid and central solenoid magnets. This is typically 200 to 350 g. The worst location is in one region near $Z = \pm 200$ cm where the component of the fringe field perpendicular to the PMT's will be about 250 g [16]. We use a 48 mm magnetic shield made from μ-metal and soft iron. This shield will protect the tube from perpendicular fields of up to 700 g. The gain drop from fields parallel to the tube axis was measured [17] and is shown in Fig. 18. A parallel field of 350 g causes a gain drop of 10%. A parallel field of 250 g causes a gain drop of 5%.

The contributers to the time uncertainty include: variation due to the resolution of the counter (two components as described above); variation in the z-position of the vertex; variation in the z-position of the counter over it's length; variation of the overall average time of collision of the bunches (long-term variation of t_0); and variation of t_0 between bunches (t_0 of each colliding bunch pair).

The front end electronics will not allow us to vary the gates to account for the time–of–flight of particles in the DØ detector at different polar angles. We will have to account for that in the lengths of the cables by making them different lengths or adding corrections.

6.3 Mounting Scheme and Space Requirements

The counters will be mounted on aluminum cross-members attached to steel brackets which are secured to the WAMUS A-Layer PDT's edges.

We have the following space requirements. The thickness of the present design of the counters is 2.75 inches, not including the mounting hardware. For planning purposes, we should reserve at least three inches of space normal to the PDT's for the $A\phi$ counters. The horizontal gap between the counters and any calorimeter component should be at least 0.5 to 1.0 inches. So the horizontal space between the counters and any central region component must be at least 3.5 to 4.0 inches.

We had the survey crew measure the space available between the WAMUS A-layer PDT's and the elements of the calorimeter. In most places there is sufficient space for the $A\phi$ counters, including the 0.5 to 1.0 inch gap. There are, however, a few modifications required.

- The smallest gap is between the cable winder/routing assembly side-channel flanges and the vertical A-layer PDT's. The plan is to move the assemblies a minimum of 1.5" towards the center of the detector. The calorimeter cables will need to be shifted slightly so that they run straight into the winder.

- The I-beam which supports the cable tray which attaches to the cable winder assemblies will also be in the way of the $A\phi$ counters. The plan is to replace the EC I-beams with channels, saving 1.5" of space. The center 1/3 of the cable try itself holds no cables and could be eliminated. The inner parts of the cable tray would then be supports by an arm which is cantilevered from the CC cradle. A smaller beam would span the distance between the support arms to provide a base for the temporary floors which we use during access. We have developed the work plan for these modifications.

- The calorimeter drop-down platforms are in the way and will have to be removable in order to close the detector. Similarly, hinges which support the platform wings will have to be modified.

- There are many minor modifications which increase the available space. For example, various studs and bolts which can be removed or shortened. Other near-misses include: the bar-stop for the "Blazey Box" on the SW preamp box; the small handles on the 1553 RMI's; the instrumentation valve on the diffusion pump labeled VP246V should be modified; the NE corner of the SW preamp box needs to be un-shimmed slightly; and a yellow manifold valve on the east side is a near-miss.

6.4 Access Issues

The counters will only be accessible when the CF magnets are in the open position. A part of the detector-opening procedure will include installtion of a false floor over the top of the A-Layer bottom counters. This will protect them from accidental damage. This false floor will have to be removed to access the counters underneath it. The side-wall counters will mostly be in arm's reach; the higher ones will be accessible from the calorimeter platforms or from short ladders. The A-Layer ceiling counters will all be accessible from the calorimeter platforms, though some may be a difficult reach over the top of the calorimeter preamp boxes.

6.5 High Voltage

The $A\phi$ system will require one HV crate, 46 Type 4 pods, and four 2X Reynolds fan-ins in the MCH. We require six Reynolds cables plus two spares and Reynolds to SHV fanouts in the E and W trusses. The counting house parts will be scavenged from the Run I tracking system. We will produce the fanouts. Each pod will supply 13 or 14 PMTs, providing a little headroom from the maximum supply current.

6.6 Aging of PMTs and Scintillator

6.6.1 FEU115 Phototubes

This was discussed in Section 5.3.2.

6.6.2 Scintillator and Fiber

The radiation dose expected in the $A\phi$ counters for Run II is also $O(10)$ rads, based on the rate measurements taken during Run I. As discussed in the corresponding section for the Cosmic Cap counters, this expected dose is orders of magnitude away from that which causes a noticable drop in light yield. Again, we will monitor the effect of radiation damage with some test fibers and plastic scintillator placed in the hottest part of the $A\phi$ system. These can be periodically removed and measured.

6.7 Survey Requirements and Plan

The $A\phi$ counter mounting system will ensure that the counters relative positions are fixed to within about one millimeter. As the counters are installed we will inspect them to ensure the counters are mounted properly. We will measure the position of each counter to 1/8" accuracy.

6.8 Commissioning

The job of integrating the sub-systems, including HV, gas-flow, cable check-out, electronics, calibration systems, and monitoring programs officially begins on October 5, 1998 when we are scheduled (see Appendix 3) to begin the commissioning of 10% of the counters over an eight week period. This date is driven mainly by the scheduled arrival of the front end electronics. In fact, this job will start sooner with the more low-level subsystems mentioned above.

The initial counter timing will be performed using the pulser system. Individual (relative) counter differences, for groups of 16 counters out of 48 in a readout card, will be removed at the ns level before the $p\bar{p}$ run starts. This will be cross-checked using beam muons. This can be accomplished using a shift-long special run providing approximately 100 muons per counter. This same calibration sample will be used to set the gate position for the groups of 16 counters as well as the overall timing gate position.

The remainder of the commissioning will take place from March 10, 1999 to September 10, 1999.

6.9 Calibration, Monitoring, and Operation

We imagine this is nearly identical to that described above for the Cosmic Cap and Bottom counters. We expect the low p_T dimuon trigger rate will be susceptible to timing shifts of a few ns. Monitoring the dimuon trigger rate as a function of luminosity provides a cross check of the overall trigger timing. Monitoring the individual contributers to the trigger rate provides a check of the individual counter timing and resolution.

We expect to take periodic special runs to monitor the individual counters timing performance.

6.10 $A\phi$ Shielding

The source of the background along the edge of the CF A-layer is the remnants of the hard collisions which hit the exit of the EC cryostat at high pseudorapidity. We will add shielding to reduce the rate of background particles which hit our central A-layer PDTs' and $A\phi$ counters.

Our initial Monte Carlo studies [18] showed that the best place to install the shielding is right in front of the detectors. A MARS Monte Carlo simulation [19] predicted a shielding factor of 5.7 ± 0.7 from 75 cm of polyethylene. In this study, a beam of MC hadrons was directed against the exit of the MC calorimeter. A prototype shield was tested during Run Ib. The reduction in rate in the prototype $A\phi$ counters was 5.0 ± 0.8. The background time-distribution was unchanged by the shielding.

Subsequently, we studied the effect of adding an iron, polyethylene, and Pb "nose shield" starting in the region 10" from the beampipe[20]. The "nose shield" has a rectangular cross section (cut perpendicular to the z-axis). The interior is a 20" wide (full width) rectangular hole for the beampipe and associated accelerator components. This is followed by a 9" thick layer of iron. The iron is followed by 6" of polyethylene and finally 2" of Pb. Different MC studies provided different answers for the effectiveness of this shielding, depending on the source of the background. Using the technique described above, we expect the "nose shield" to reduce the rate by a factor of 4.6 under Run I levels. The addition of the polyethylene donut improved the rate by only a factor of 1.2. Using DTUJET minbias events instead of a fixed hadron beam, the "nose shield" only improved the rate by a factor of 2.1 ± 1.0. The addition of the polyethylene shield improved that by only 1.1 ± 0.1. In both cases the polyethylene shield is predicted to have little effect once we have a "nose shield".

The design work for the shield is concluded. It would have been assembled from high-density polyethylene plates cut to shape. Figures 19 and 20 show a front-view and side-view of the shield. We studyed the feasibility of using polyethylene doped with Lithium. Li_6, which comprises about 7% of the natural Li, has a high cross section (n,α) reaction and is thus an especially good neutron absorber. That would not have fit within our budget.

Given that the effect of the polyethylene donut is predicted to be small. We don't plan to build it. Once we have collisions with the "nose shield" in place, we will test the potential effectiveness of augmentations.

7 Conclusion

This report has detailed all of the major technical design issues for the central muon system upgrade. The muon upgrade design is driven by the observation that the proportional drift chambers used in Run I deteriorate too rapidly with integrated luminosity to be used in the forward region in Run II. In the central region, we will retain the present drift tube system, complete the scintillator coverage around the outside of the toroid magnet, and add an additional layer of scintillation counters in front of the toroid magnet to increase the trigger capability. The $A\phi$ polyethylene "donut" shield may not be very useful if we have the iron, polyethylene, and Pb "nose" shield. While we have a design, we don't believe we will need to build it.

Appendix 1: Calibration and Monitoring Systems – General Description

The diagnostics and calibration system for the Run II Muon Detector has three goals: to determine if the muon detector channels are operational, to determine calibration constants, and to test the muon trigger system. Each of the detectors requires a slightly different set of calibration studies but the similarities are large enough that the system can be discussed in a general way.

By the nature of the readout electronics for the muon system there are four levels of system testing progressing from the simplest to the more complicated, depending on the amount of the DAQ involved in the test. They are:

1. Front End Level - requires detector/pulser + FEB/SFC + Control Card
2. Crate Level - requires detector/pulser + FEB/SFC + Control Card + Readout Crate (MRC)
3. Host Level - requires Crate Level + VI + Host computer
4. DAQ Level - requires Crate Level + VBD + Level 3 + Trigger Framework + DAQ.

At the Front End Level, the digital signal processor (DSP) on the Control Card will perform the processing. At the Crate Level, the 68k computer will do the processing. For each of these levels, a host computer will interface with the Control Card or the 68k via an RS-232 port. At the third level, a host computer will also upload the data via the VI (Vertical Interconnect) to perform the analysis. At the DAQ level, the entire DØ DAQ structure will be used to deliver the data to a host computer. During Run I operation we used the last three levels of monitoring. They were known as Mu_Local, DAQ_Local, and Calib, respectively.

The Crate Level and Host Level system tests require the detectors to have self-triggering capability for individual channels. For example, for the WAMUS PDT's, there will also be the ability to trigger on n-deck coincidences (n=0,1,2,3,4). The Front End Level tests work with either self-trigger or an external trigger, such as generated by the Trigger Framework. Each control card will have an external trigger input allowing trigger from any other external source. The DAQ Level tests use triggers generated by the Trigger Framework.

The information for these tasks will be accumulated with pulser systems between stores, from cosmic ray muons, and from data taken with beam. Details of the measurements needed for each system have been included in the corresponding subsections.

The pulser systems will serve to determine and monitor the calibration constants. In addition, they will decouple the detector elements from readout electronics failures. Furthermore, they will also be useful to test the muon triggers; this will be done by downloading masks to generate trigger patterns.

Each of the front end cards will be pulsed by a variable amplitude, variable delay analog pulse which is generated by the Controller card for the readout crate. The pulse will always appear at the input of the card so as to best simulate a signal from the chamber.

To decouple the scintillator PMTs from the SFCs, an LED pulser system will be used. This system will also serve to quickly find dead PMTs, monitor PMT gains which most strongly affect trigger timing, and track timing and threshold changes. It is described in detail in a separate document[22].

Appendix 2: Cost Estimate

Appendix 3: Schedule

References

[1] "The DØ Upgrade", DØNote 2542, Fermilab-FN-639 (April 1995).

[2] "The Standard Model and Beyond: Physics with the DØ Experiment", DØ Collaboration, Fermilab-FN-640, (December 1995).

[3] "The DØ Upgrade: Forward Preshower, Muon System and Level 2 Trigger", DØNote 2894, Fermilab-FN-641 (March 1996).

[4] "The DØ Detector", Nucl. Instr. and Methods, A338, 185 (1994).

[5] "Magnetic Field Calculations", DØNote under preparation by Cullen Nicholson.

[6] "Study of Fast Gases, Resolutions, and Contaminants in the DØ Muon System", J. M. Butler et al., Nucl. Instr. and Methods in Phys. Res. **A290**, 122 (1990).

[7] "Crud Removal from Muon Drift Chamber Wires Using *ZAP* Cleaning", T. Marshall and H. Haggerty, DØNote 2556, (June 1995).

[8] "Design and Test of the WAMUS Service Card and Jumper Board", under preparation by H. Haggerty.

[9] "Scintillation Counters for the DØ Upgrade", A. Ito et al., Elsevier Preprint, (October 1996).

[10] "Design Desription for the CF Bottom B-Layer Scintillation Counter and Support Frame", H. Cease *et al.*, DØNote 2731, (July 1995).

[11] H. T. Diehl and A. S. Ito, "Central Muon Upgrade Cosmic Side Wall Gap Counters", DØNote 3355, (November 1997).

[12] S. Majewski, R. Wojcik, and D. Weisenberger, "Studies of a FEU-115M Photomultiplier", CEBAF Note (June, 1993).

[13] "A Study of the Long-Term Gain Dependence of Phototubes", B. Pope, DØNote 2451 (January 1995).

[14] S. Gurzhiev and V. Evdokimov, Reports presented in DØ Muon Upgrade Meetings, (Sept. 1996 - Nov. 1996).

[15] S. Gurzhiev, "Aging of Forward Scintillator and Fiber under Radiation", Report presented in DØ Muon Upgrade Meeting, (Sept. 13, 1996).

[16] R. Yamada et al., "Proposed Correction Methods for Fringing Field of 2 Tesla Solenoid on Main Ring Beam", DØNote 1888 (September 1993); R. Yamada, private communications.

[17] S. Gurzhiev and A. Kostritsky, "Suceptibility of FEU115M PMT's to Magnetic Fields of Various Orientations", Reports presented in DØ Muon Upgrade Meetings, (Sept. 1996 - March, 1997).

[18] H. T. Diehl and S.C. Eno et al., "Proposal for Central Muon A-Layer Scintillator Trigger Counters", DØNote 2213 (January 1995).

[19] H. T. Diehl et al., "Test of a Polyethylene Shield for the Central Muon A-layer Upgrade", DØNote 2685 (August 1995).

[20] H. T. Diehl, "CF A-Layer Shielding Studies", Report Presented in DØ Muon Upgrade Meeting, Feb. 20, 1998.

[21] "Muon Chamber Alignment", H. Johari, W. Smart, A. Taketani, and T. Yasuda, DØNote 2279, (September 1994). "Alignment of the DØ Detector", W. Smart, DØNote 2909, (April 1996).

[22] "LED Pulser System for the Muon Upgrade Scintillation Counters", P. Hanlet et al., DØNote 3XXX, (October 1996).

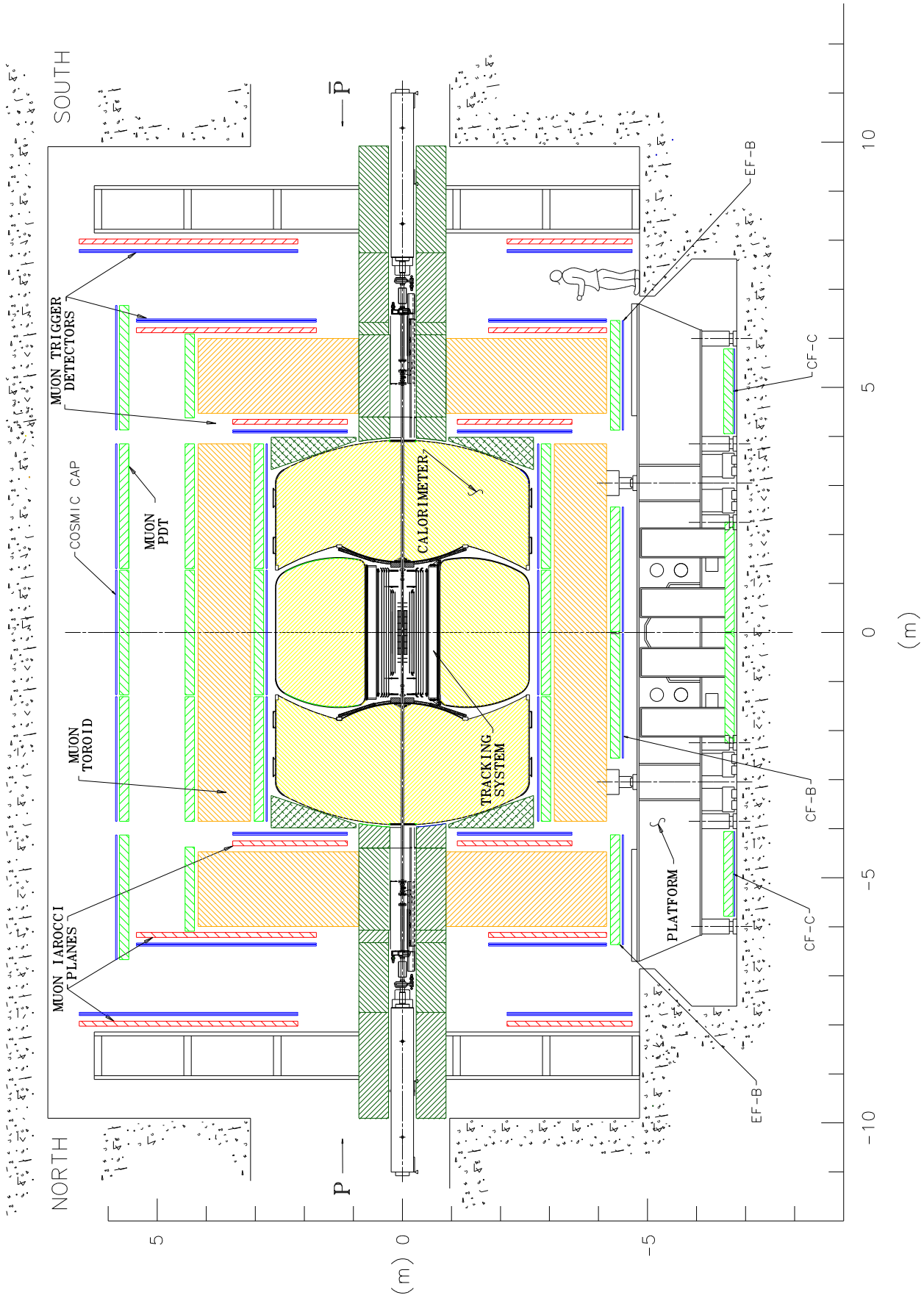

Figure 1: Plan view of the upgraded muon detector.

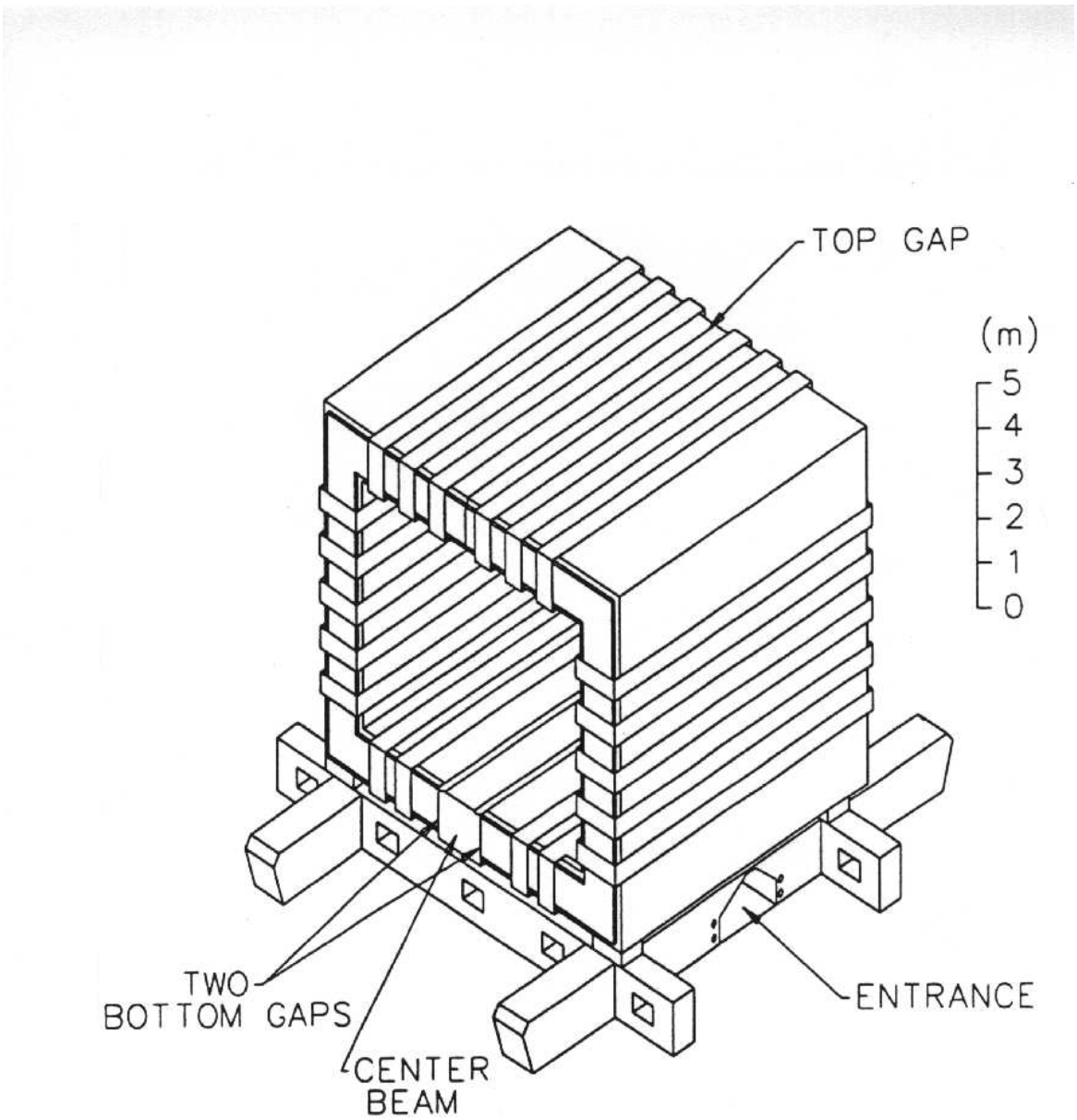

Figure 2: View of the central muon toroid showing the coils, the center beam, and the seams for opening and closing the detector.

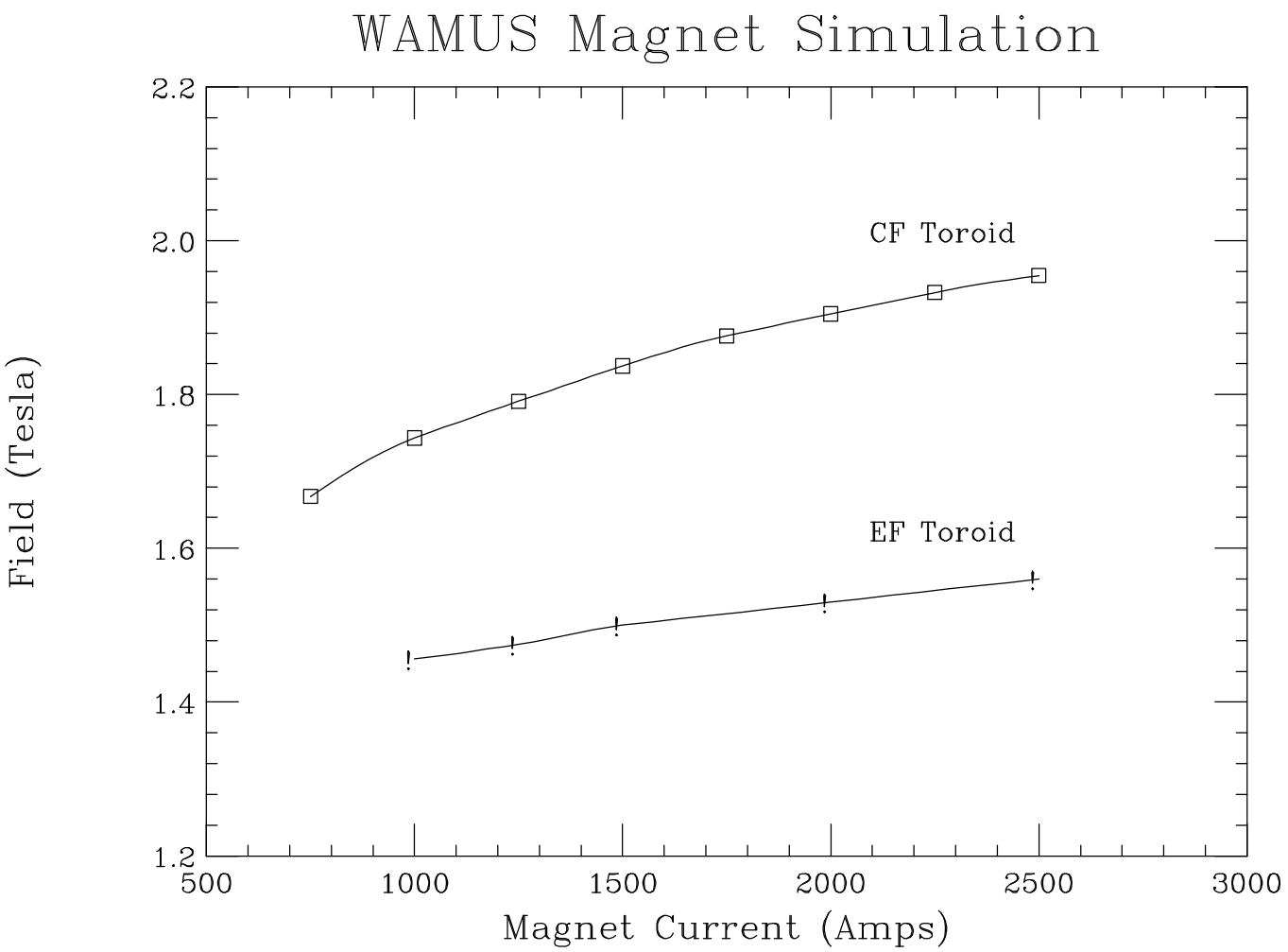

Figure 3: Magnetic field of the central and forward muon toroids plotted against the magnet current.

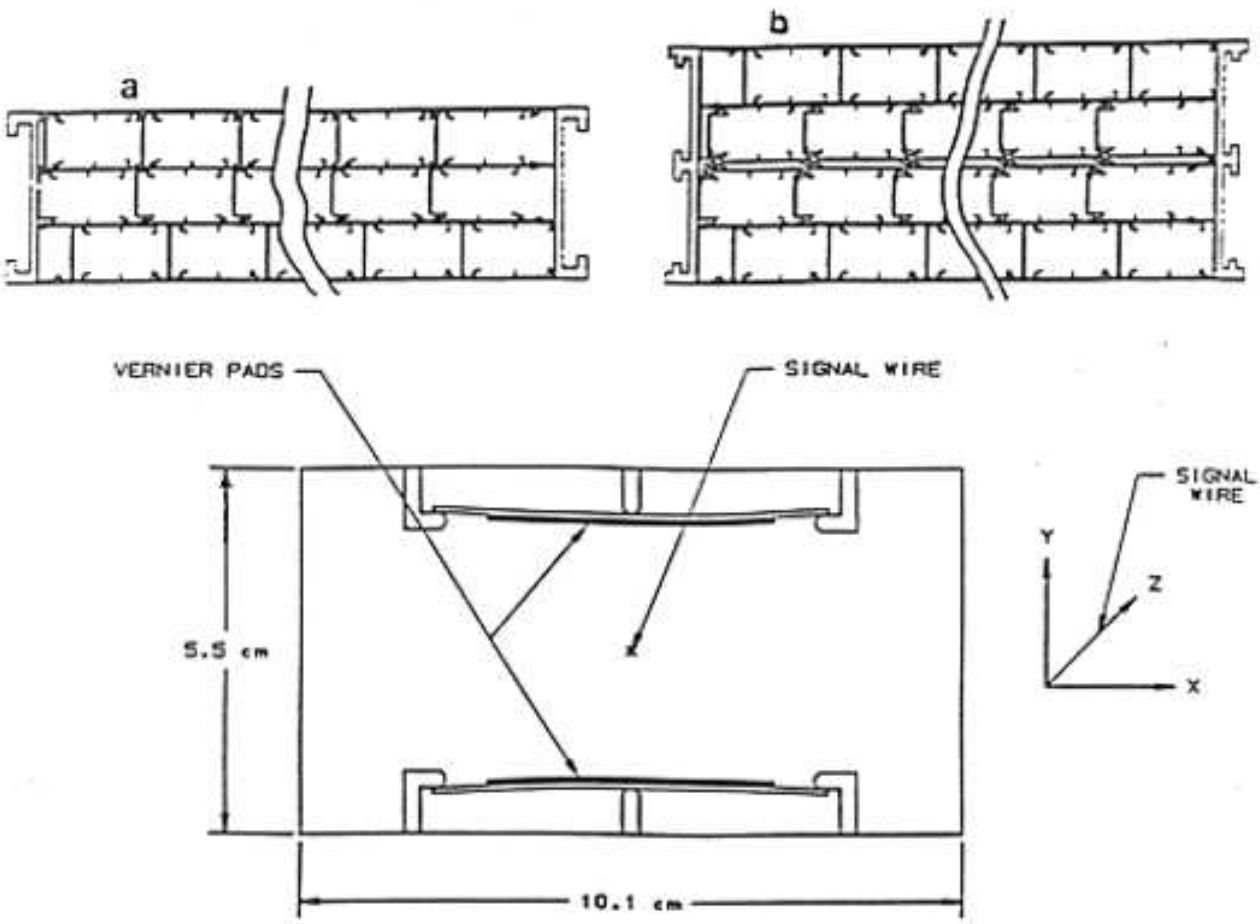

Figure 4: Wamus. Fig (a) is the end view of the 3-deck extrusion. Fig. (b) is the end view of the 4-deck extrusion. The larger figure shows the end view of a single cell, in cluding the cathode pad.

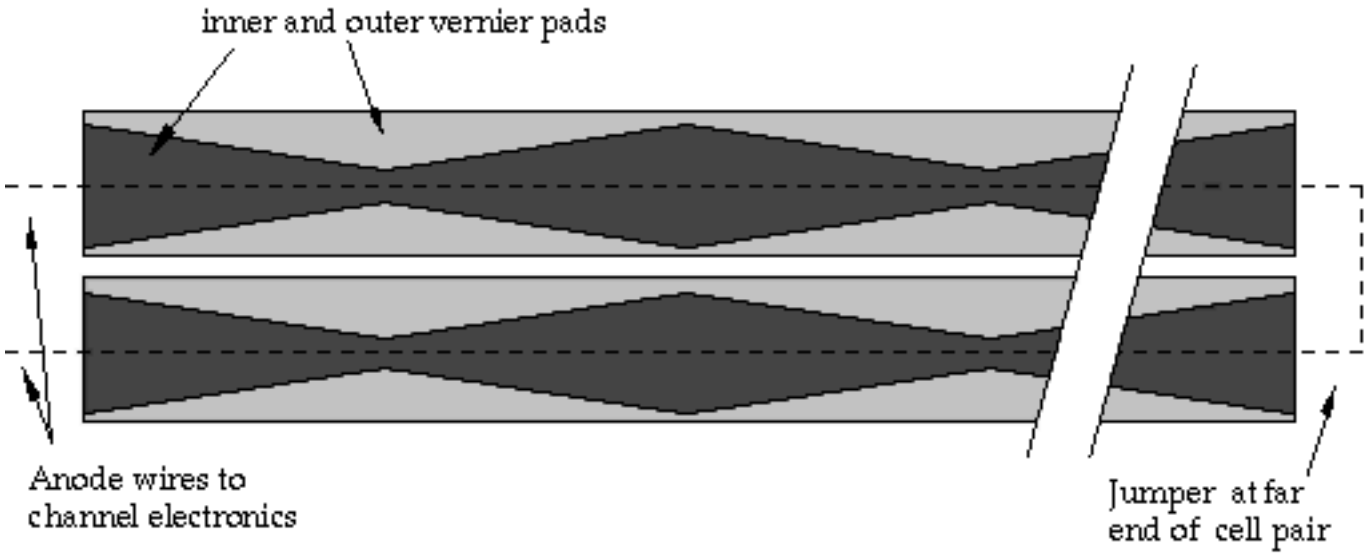

Figure 5: Wamus pads viewed from above.

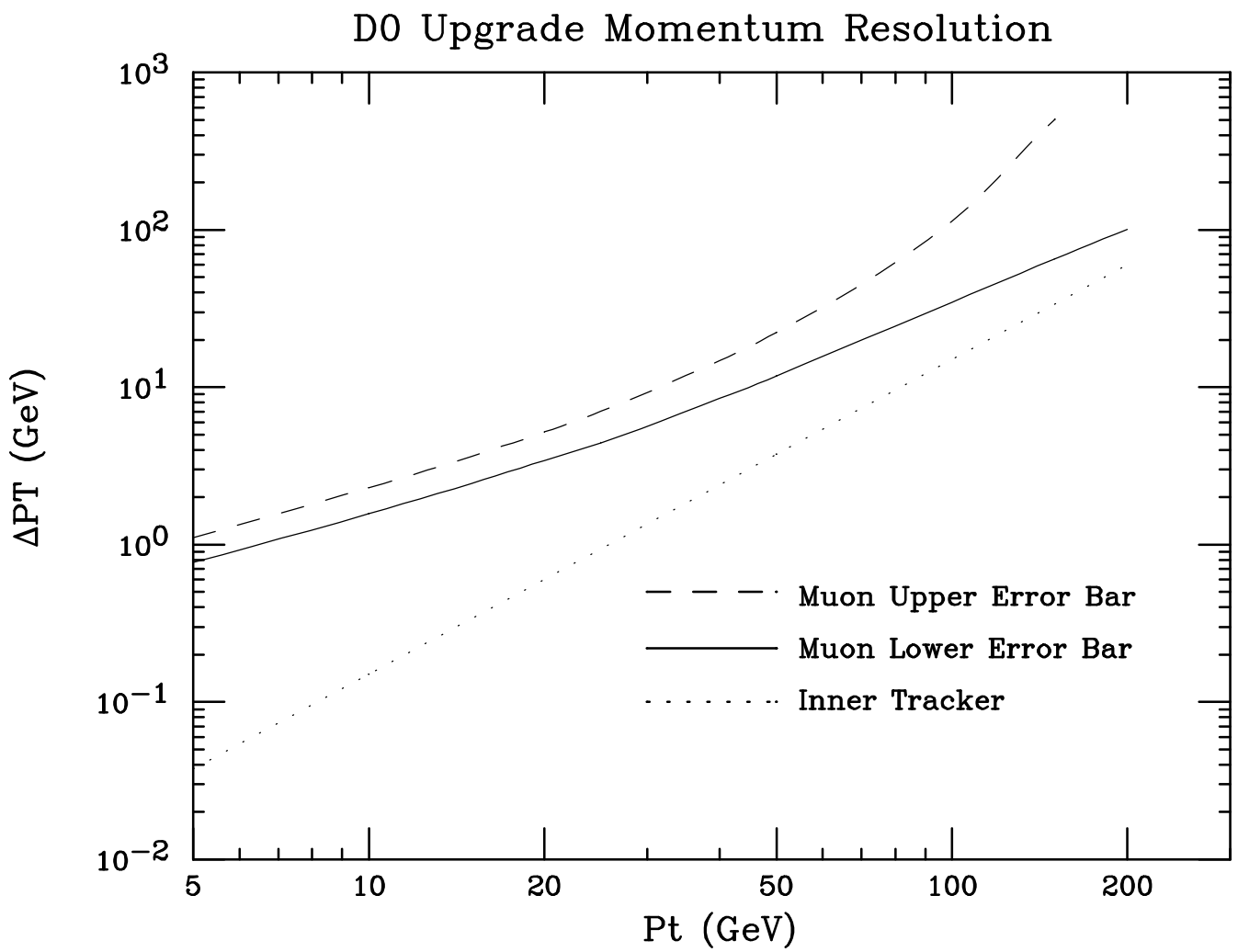

Figure 6: Momentum resolution of the muon system compared to the SFT. Notice the fiber tracker is alway better than the central muon system.

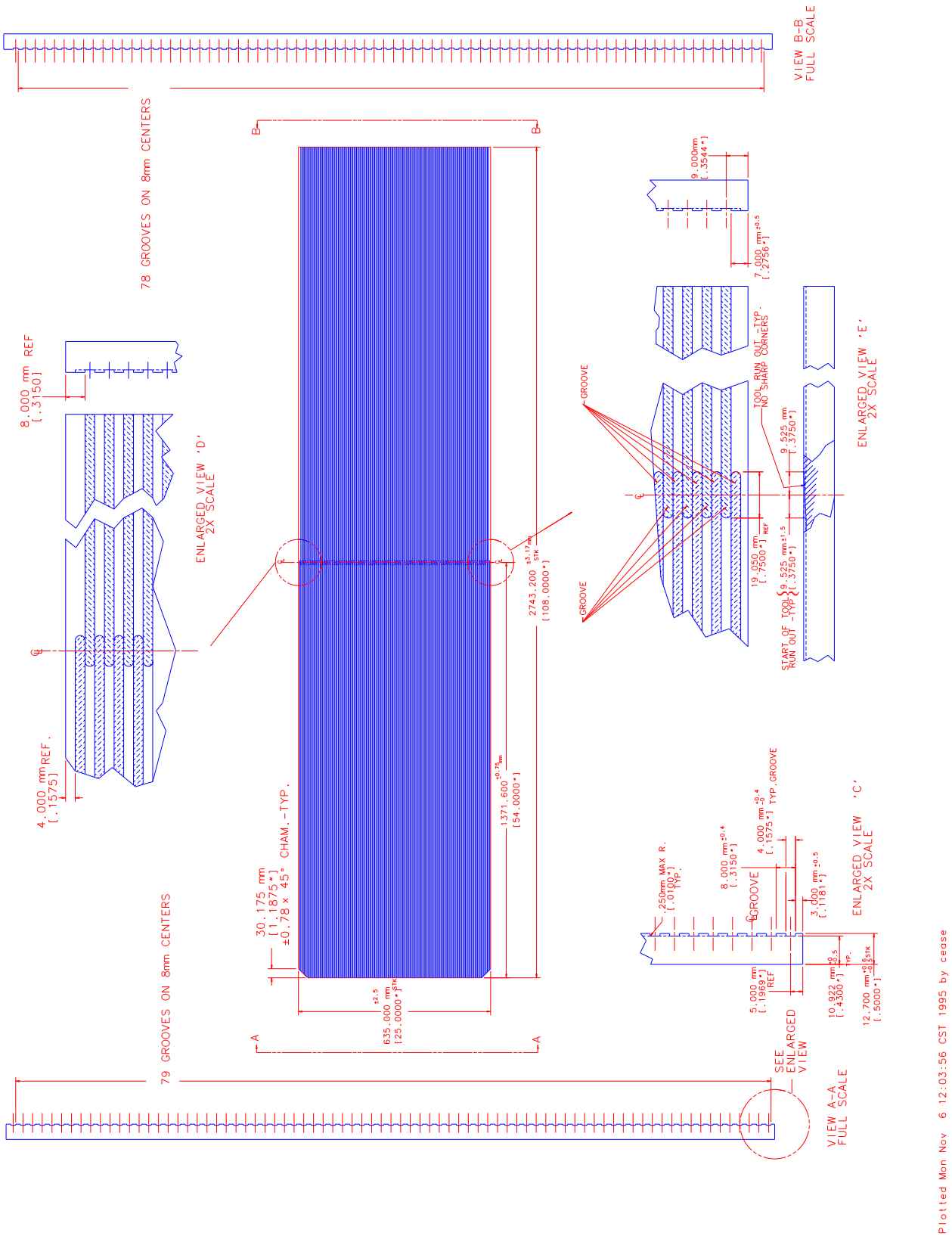

Figure 7: Detail of fiber layout for the CF Cosmic Cap counter.

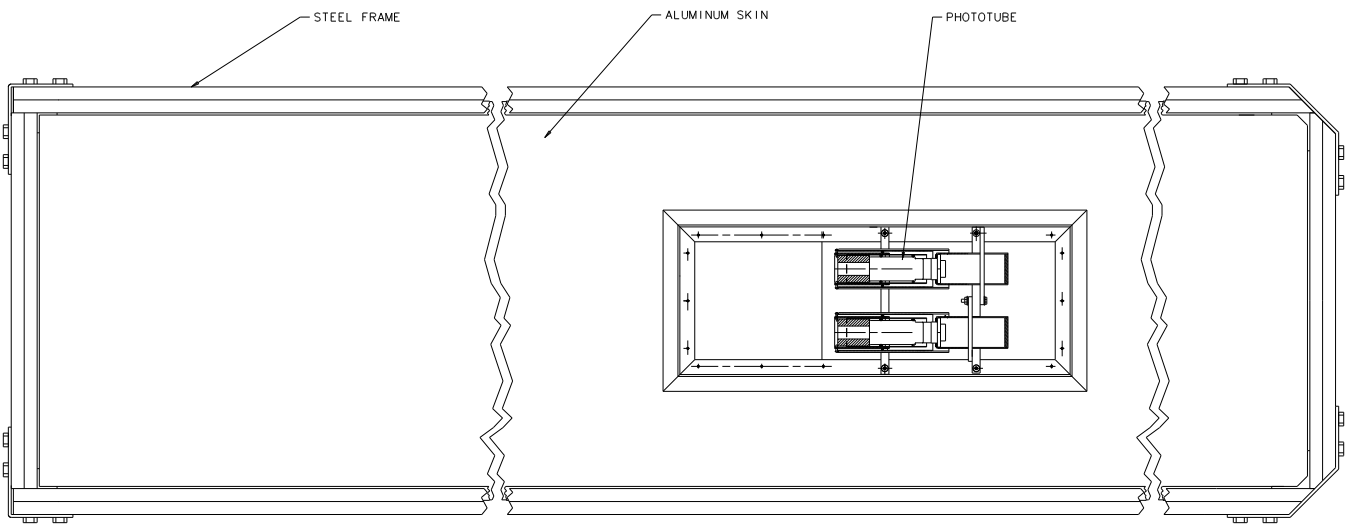

Figure 8: CF Cosmic Cap counter assembly top view. This shows the appearance of the counter as seen with the PMT cover removed.

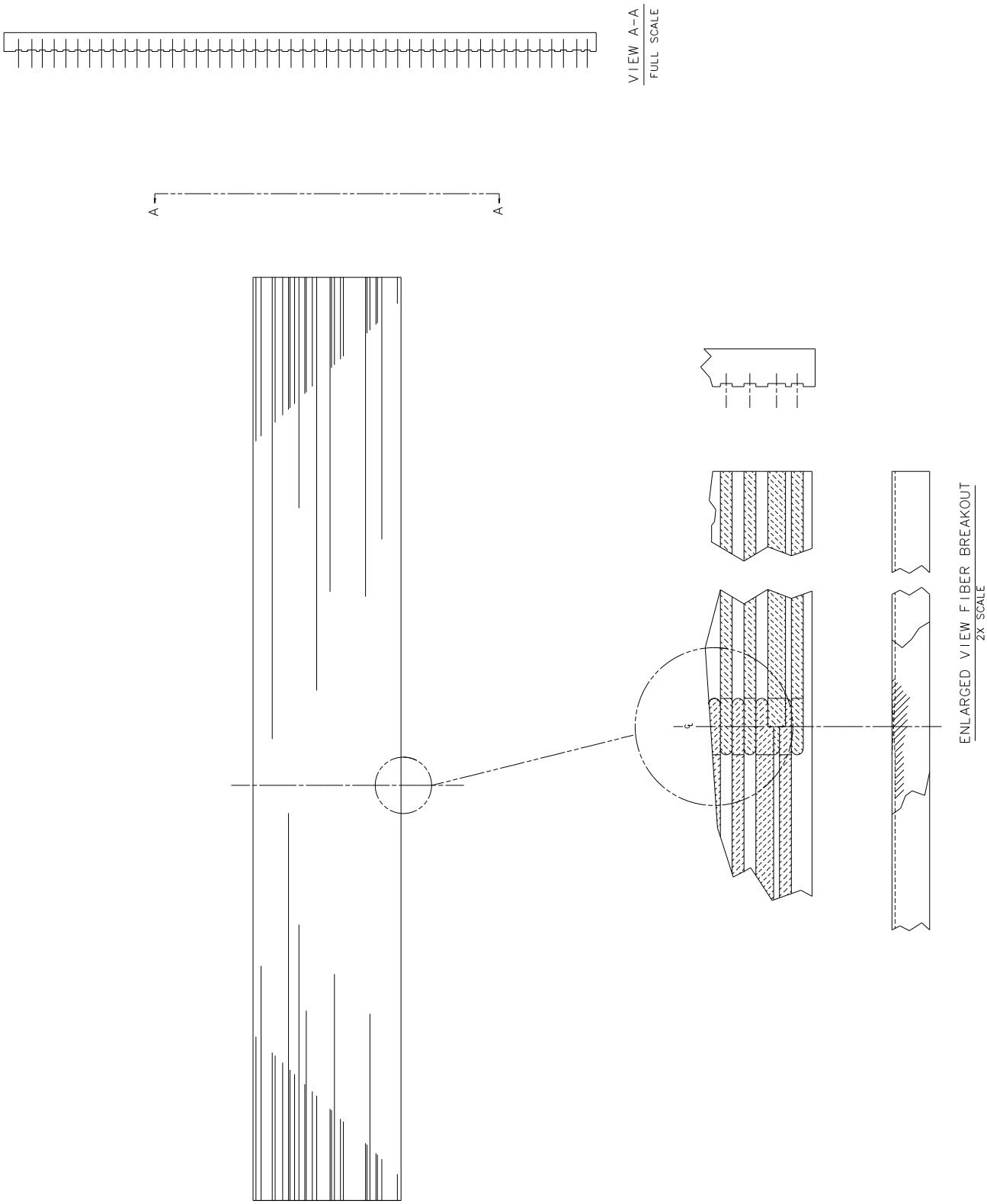

Figure 9: Detail of the fiber layout for the CF Bottom B counters.

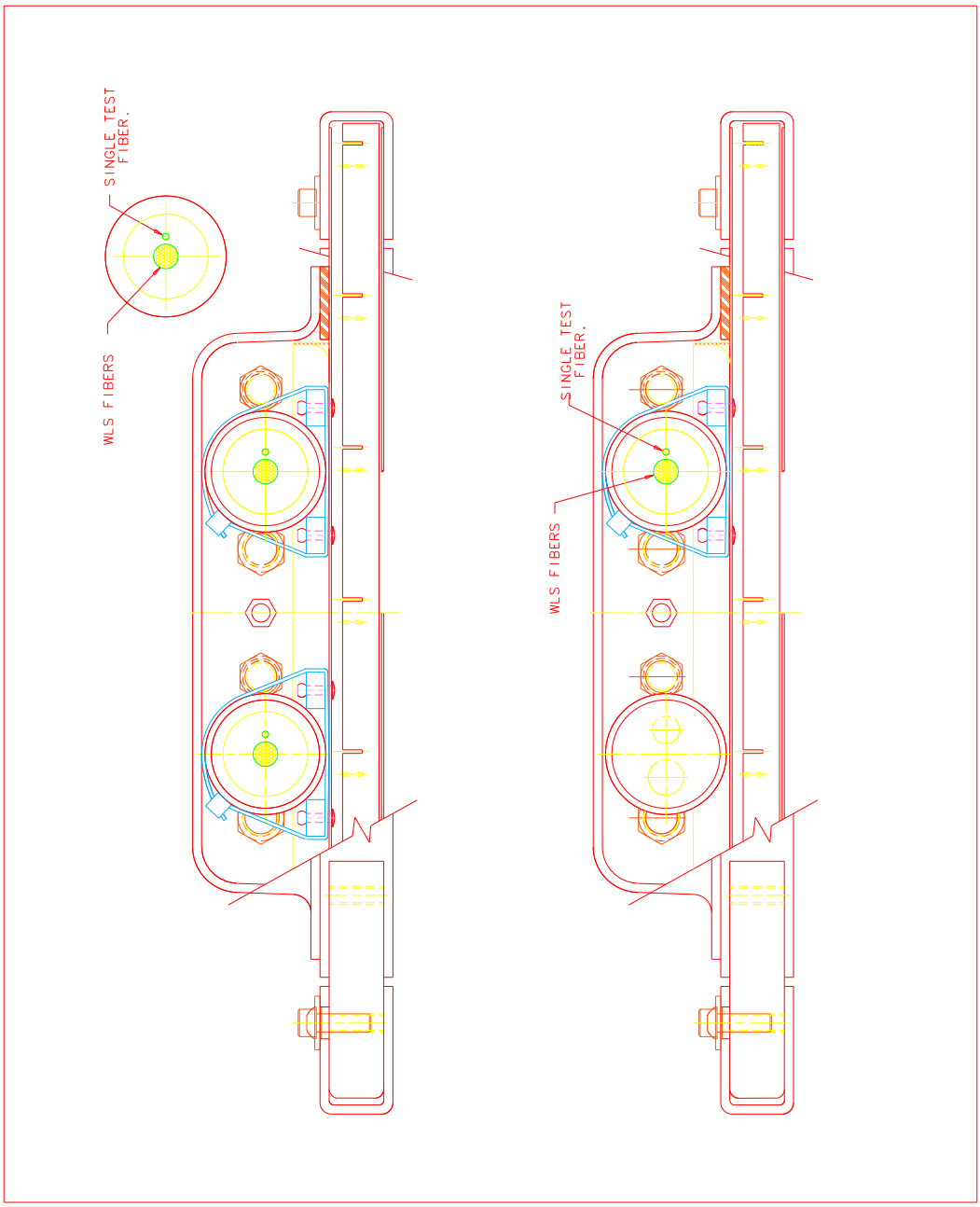

Figure 10: EF Bottom B counter assembly. Notice the grooves in the scintillator are oriented vertically.

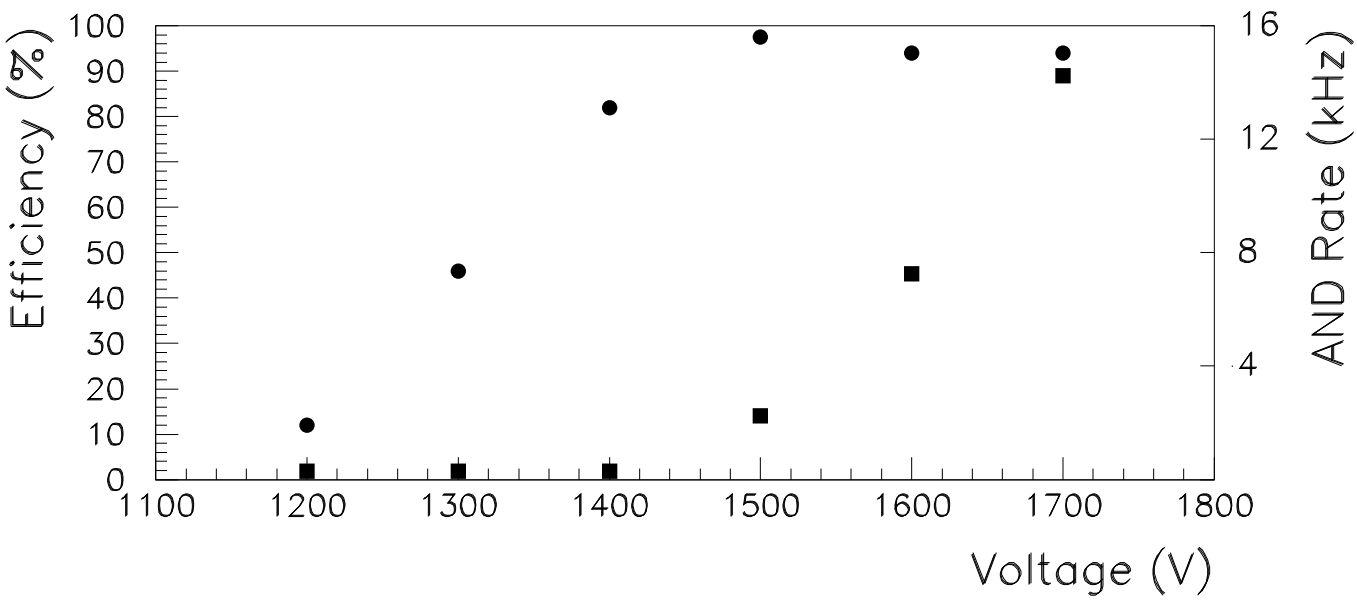

Figure 11: Efficiency and AND rate vs. voltage for a Cosmic Cap counter operated in Run I.

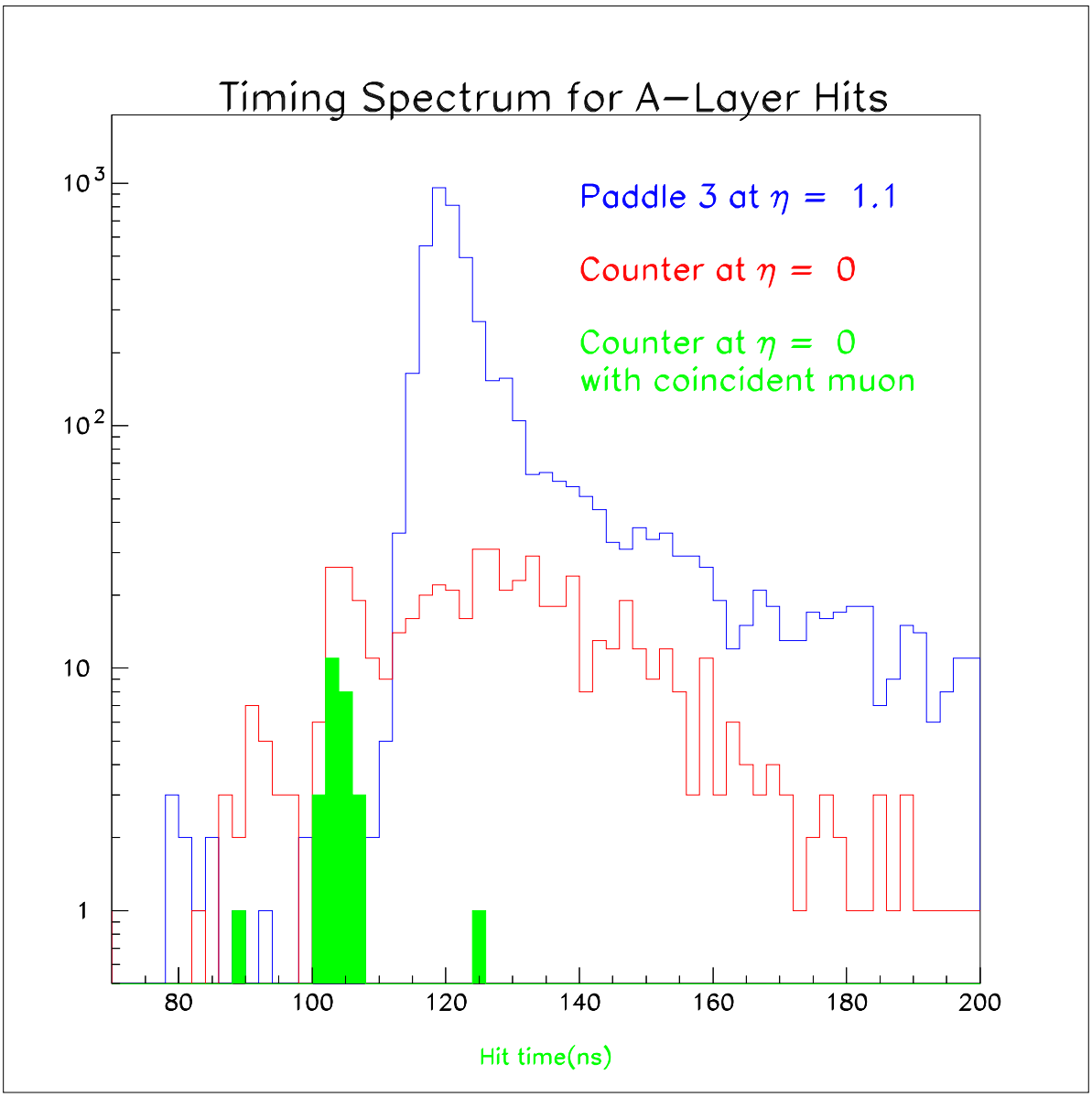

Figure 12: Timing spectrum for prompt muons and out-of-time background in two early prototype $A\phi$ counters operated in Run I.

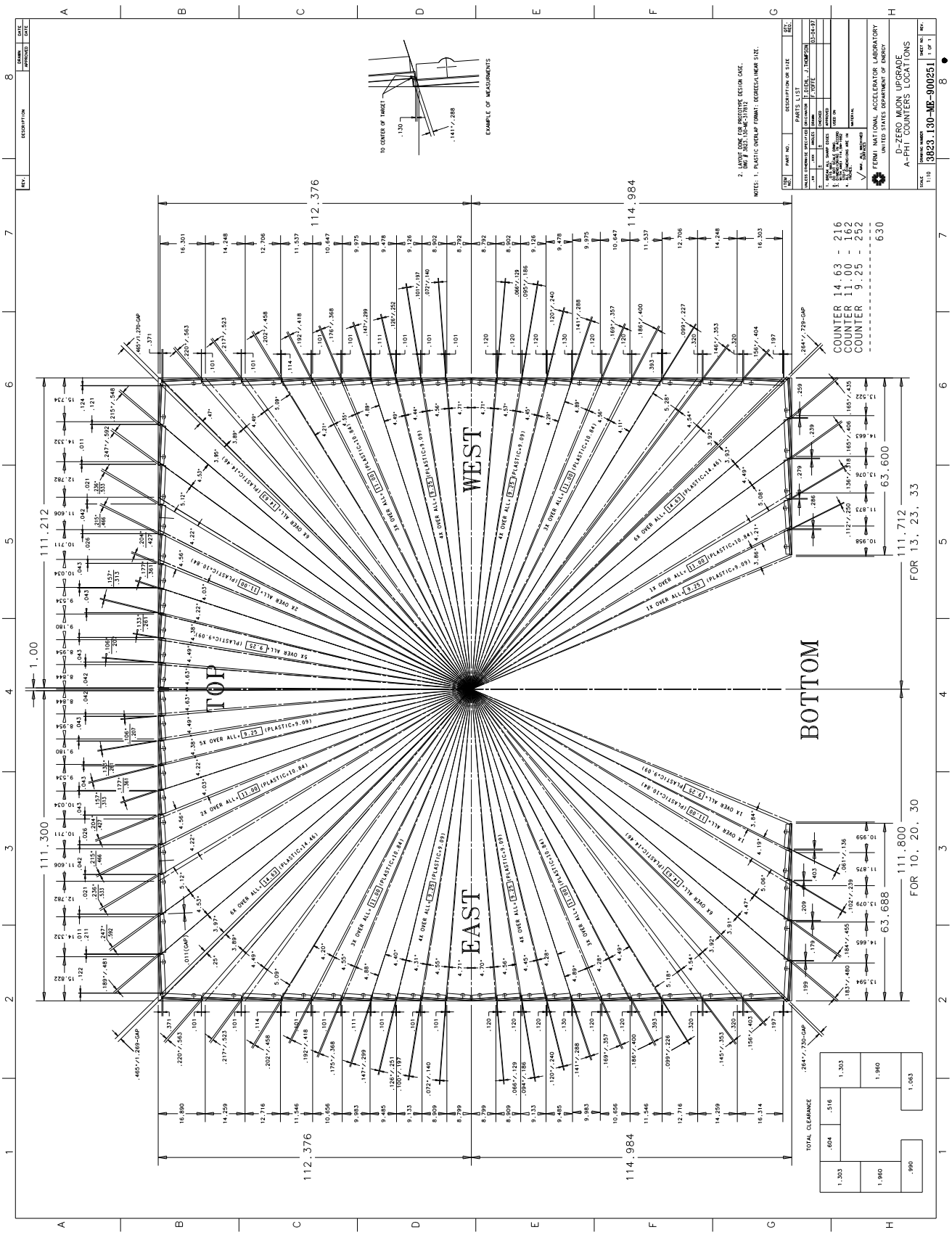

Figure 13: Layout of the A-Layer counters.

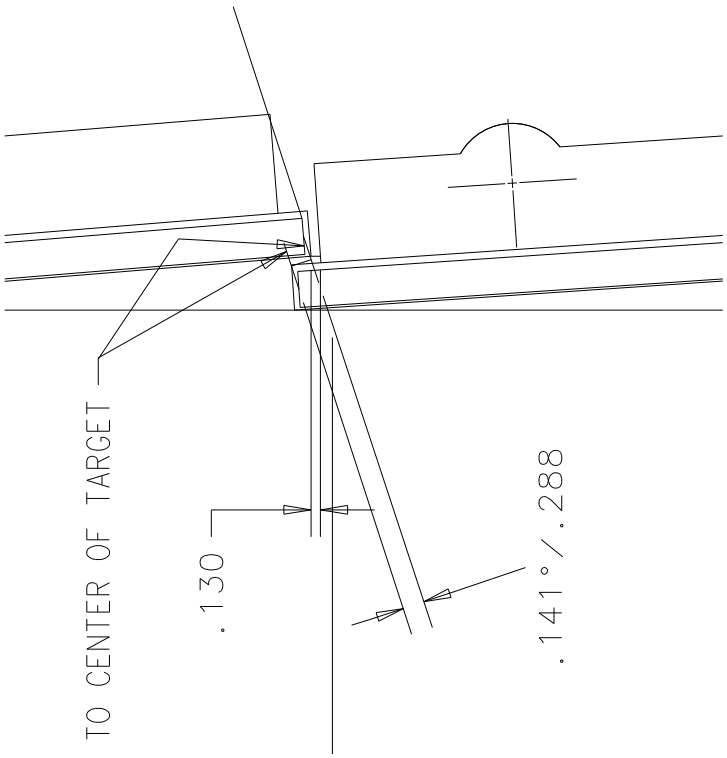

Figure 14: Detail drawing of the overlap of two A-Layer counters.

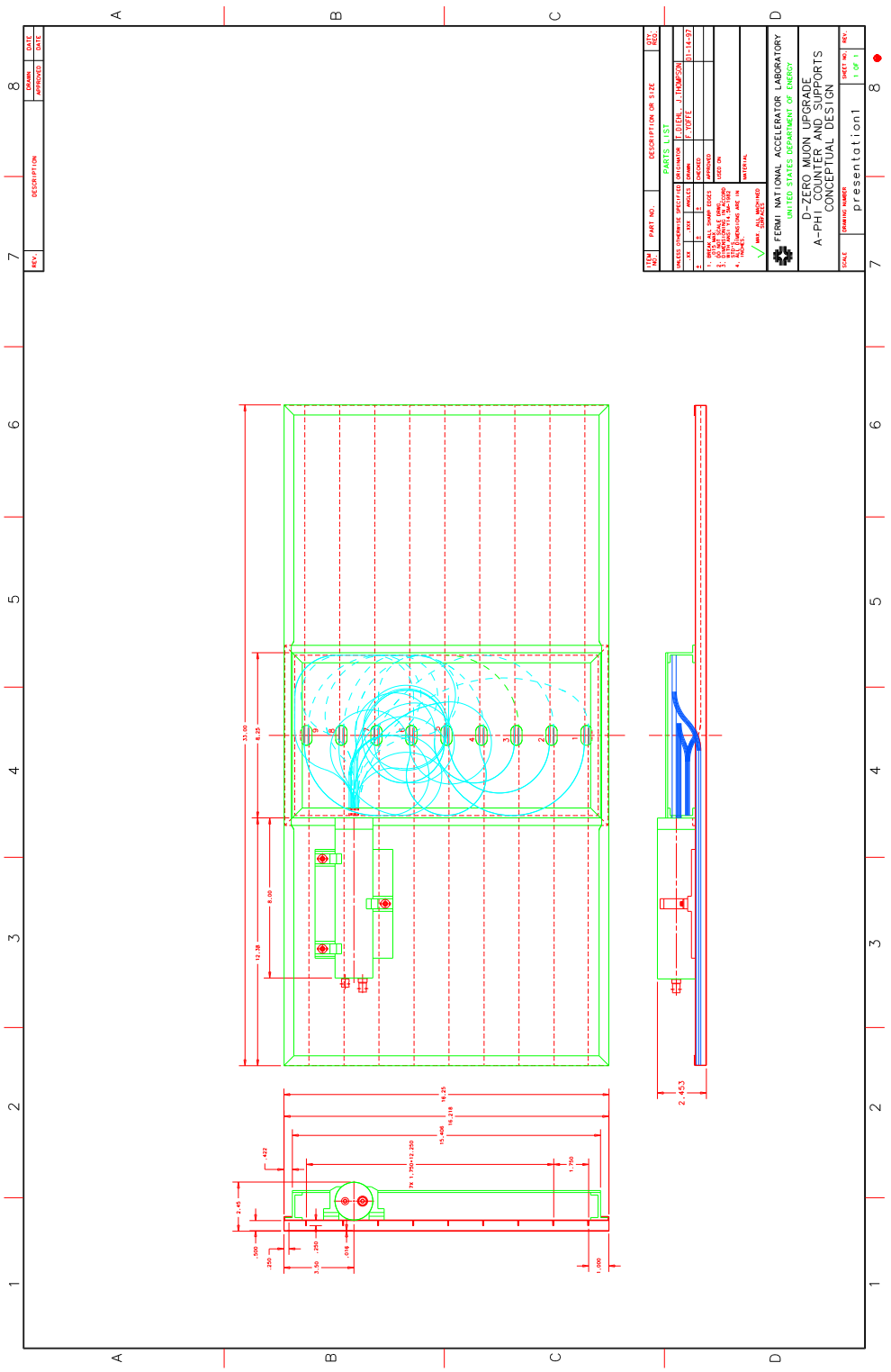

Figure 15: The design of the latest prototype $A\phi$ counter.

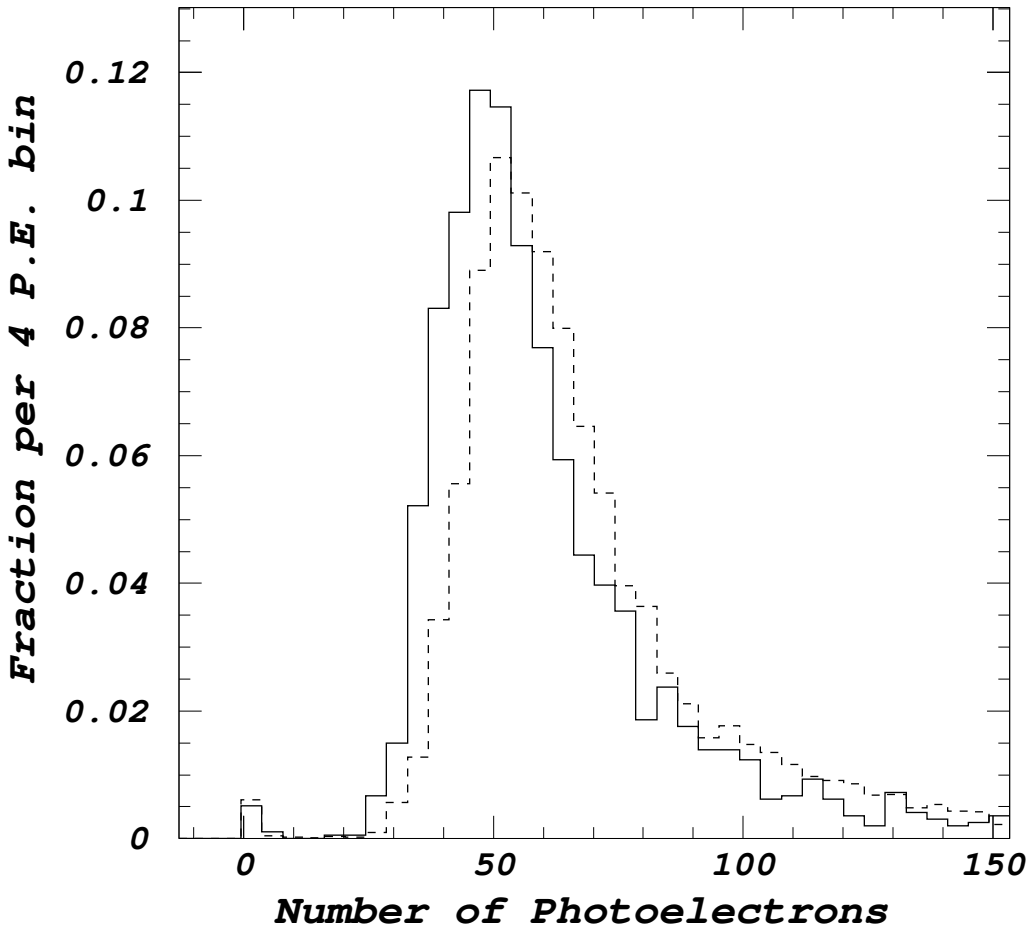

Figure 16: Amplitude spectra for Aϕ counter prototype. Solid histogram corresponds to the area along the short edge of the counter, dashed histogram - to the area in the middle of the counter. Events near zero are due to random noise in trigger counters.

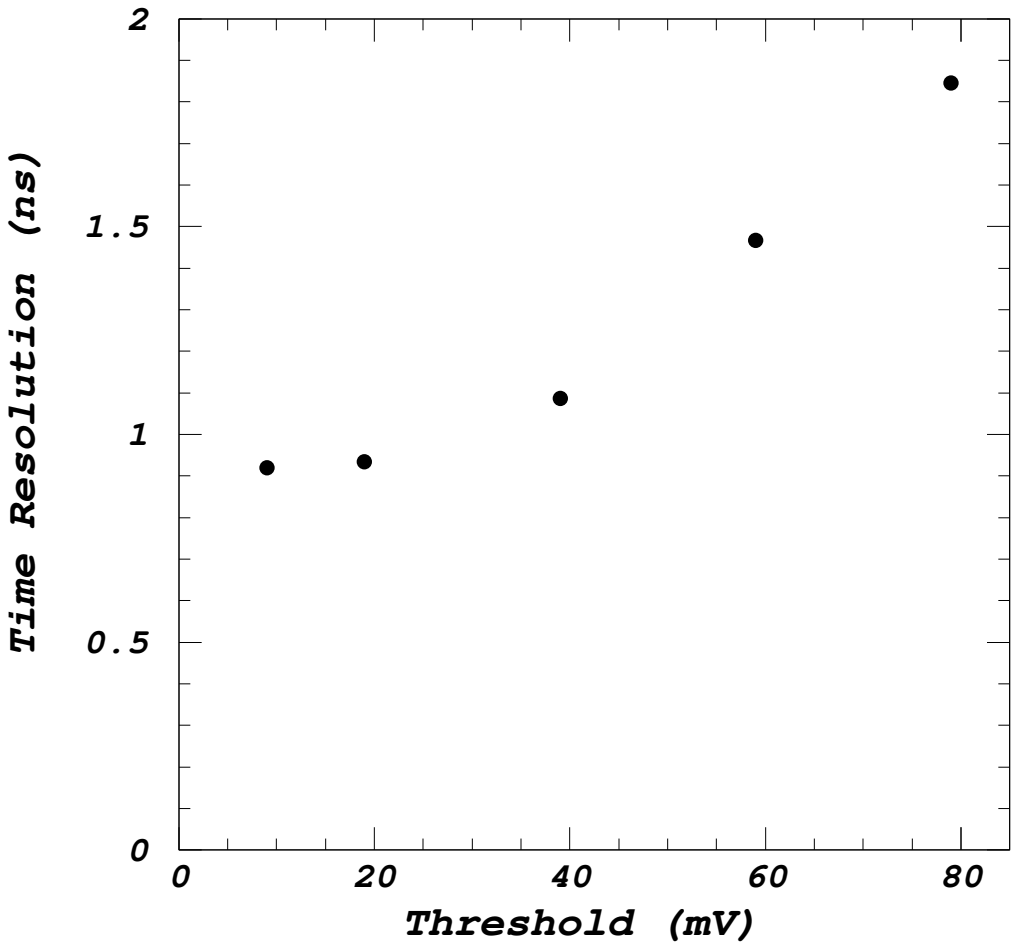

Figure 17: Time resolution of Aϕ prototype as a function of threshold.

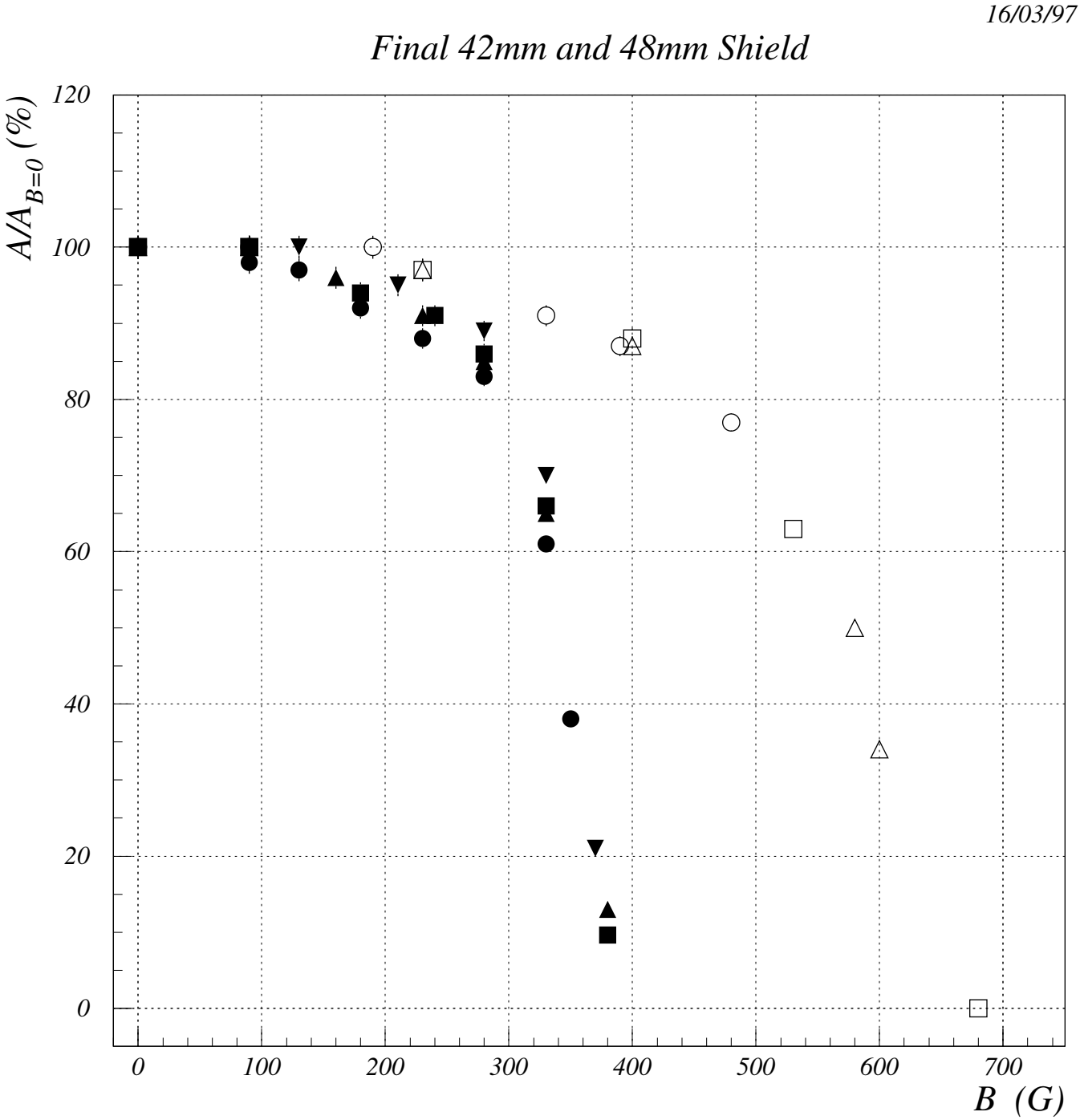

Figure 18: Relative gain change of several 115M PMT's in magnetic fields parallel to the tube axis. Open circles, squares, and triangles are with a 48 mm magnetic shield; closed circles, squares, and triangles are with a 42 mm magnetic shield.

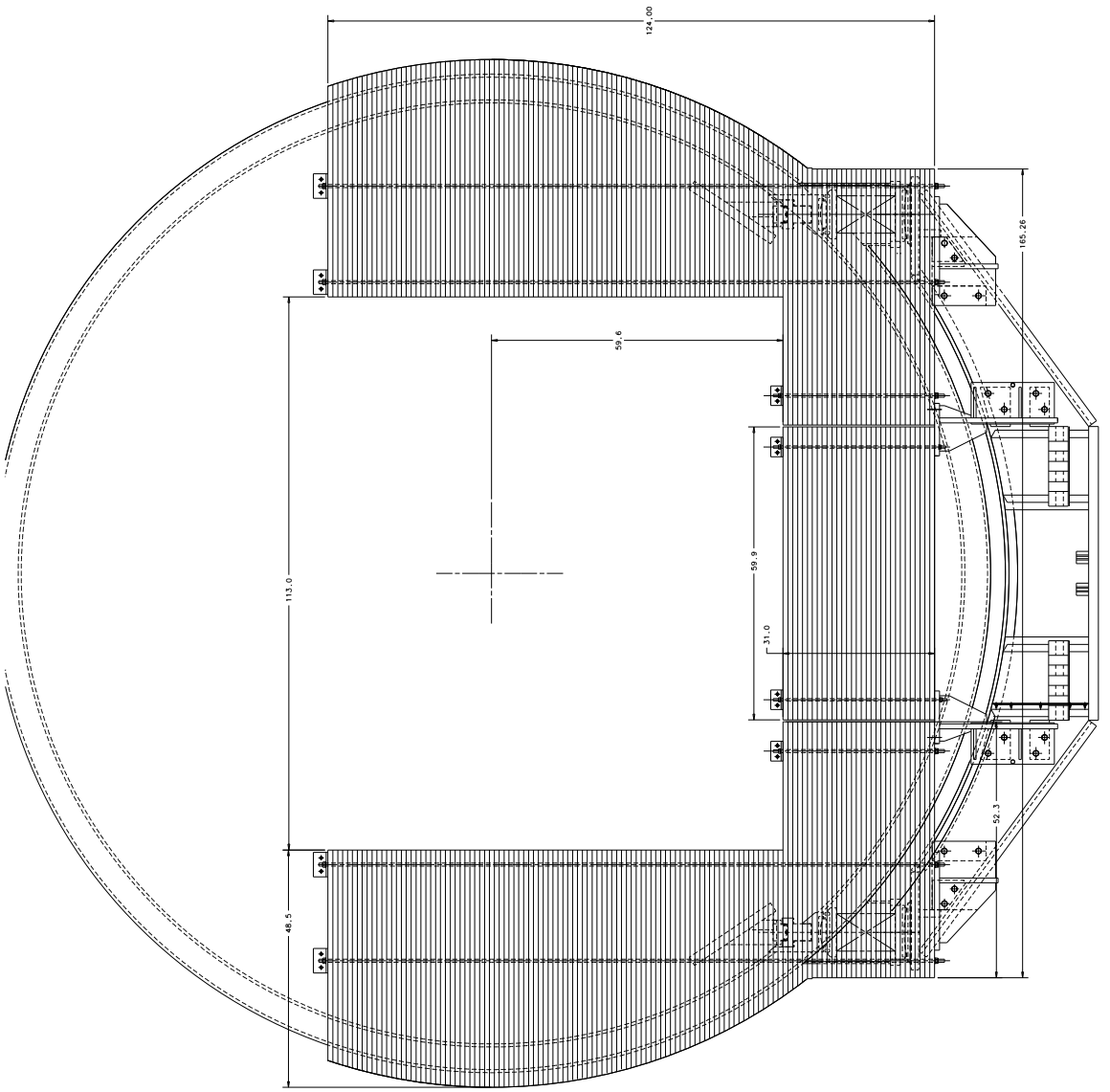

Figure 19: End view of the A-Layer shield.

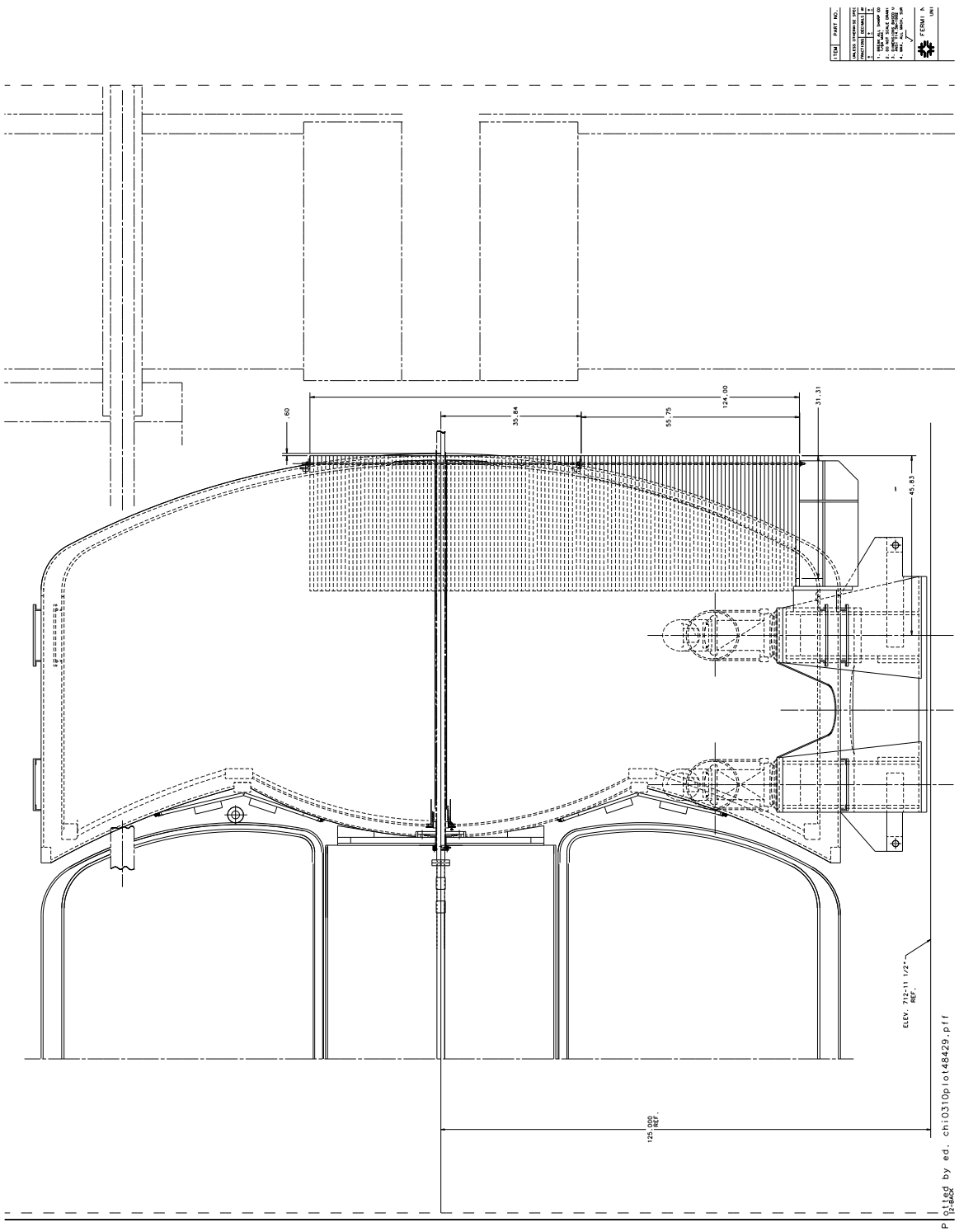

Figure 20: Side view of the A-Layer shield.